Sodium hydroxide substitution in slag activating mixes: A potential pathway to more sustainable slag-based binders

Ugo de Filippis, Elodie Prud'Homme, Sylvain Meille

Sodium hydroxide substitution in slag activating mixes: a potential pathway to more sustainable slag-based binders

Ugo De Filippis[a], Elodie Prud'homme[a,*], Sylvain Meille[a]

[a] Univ Lyon, INSA Lyon, UCBL, MATEIS UMR 5510, 7 avenue Jean Capelle, 69100 Villeurbanne, France
*Corresponding author: elodie.prudhomme@insa-lyon.fr

Alkali-activated slag is commonly used as a cement substitute to reduce the environmental footprint of construction materials. Nonetheless, the use of significant amount of alkaline activators, such as sodium silicate or sodium hydroxide, can be detrimental in terms of global warming potential impact. The aim of this work is to use complementary activators as partial replacement of sodium hydroxide, and therefore reduce the environmental footprint of the activated slag binder. Calcium hydroxide, calcium carbonate, calcium sulfate and magnesium oxide are used as complementary activators in binary or ternary activating mixes. The compressive strength at 28 days are higher (up to 18%) for the calcium carbonate and calcium sulfate-activated samples as compared to the reference activated with sodium hydroxide only. The characterization of the microstructure shows that the proportion of activated slag and the nature of hydrates formed depend on the nature of complementary activators. Calcium aluminum silicate hydrates and hydrotalcite are favored by the presence of calcium carbonate and magnesium oxide, and a sodium calcium aluminum sulfate hydrate is formed in the presence of calcium sulfate. The life cycle impact assessment (LCIA) performed on the different formulations shows that a partial substitution of sodium hydroxide is a potential option to develop more sustainable slag-based binders.

Keywords: Activator Mix, Slag hydration, Hydrates assemblage, Microstructure characterization, Life cycle assessment (LCA)

1. Introduction

In the search for the production of more sustainable construction materials, alkali-activated slag is widely studied for its potential as an alternative to Portland cement. The main benefit of this substitution is the reduction of the environmental footprint of the produced materials, mainly in terms of global warming potential (as $CO_{2\text{-eq}}$ emissions) [1–4]. However, the mechanical and chemical properties [3,5–11] and the environmental impact [1,4] of cements produced from alkali-activated materials largely depend on several factors including the nature and amount of the activator used [12]. Nowadays, the mainly used activators are sodium hydroxide and sodium silicate [11,13] which notably affect the environmental impact of alkali-activated slag [2,14–17]. This negative impact is mainly due to their production process. Sodium hydroxide production consumes high amount of electricity for electrolysis process and the production of sodium silicate involves heating a silica source (mainly silica sand) with soda ash or sodium hydroxide at high temperature [18]. Finally, the use of highly alkaline solution involves handling and usage issues as well as possible leaching to take into consideration. The search for alternatives in the activating mix is then of great interest to further enhance the interest of using these materials. In this respect, the use of alternative activators, such as sodium carbonate [6–8,19–22], calcium carbonate [23] or sulfates [24–26], has been studied. Nonetheless the modification of the activating mixture strongly impacts the hydration process, the microstructure and the final properties of the hydrated slag.

Likewise Portland cement, the hydration of slag consists of three stages: surface dissolution of initial anhydrous grains, increase of the concentration of dissolved species in the vicinity of the grains and precipitation of hydrated phases once the concentration reaches the solubility limit. The precipitation of new phases consumes the dissolved species, reducing their concentration, allowing further dissolution of the grains [17,23,27–30]. The main difference between the hydration of slag and Portland cement is that the latter is easily dissolved in pure water whereas the former is not [23,31]. Thus, the rate of reactivity of slag in pure water is very low [23]. This is the reason why an activator is needed to enhance the initial dissolution of slag grains. Alkali metals are particularly effective to initiate slag dissolution because of their ability to break the initial glassy structure of slag by weakening the Si-O-T (T standing for Si or Al) bounds thanks to their high polarizing power and high affinity for the bridging oxygens [32]. Besides, they provide basic activating solution with high pH values, which favors hydrolysis of the initial glassy network [17,28]. The higher the pH value, the higher and faster the dissolution of acidic silicate and aluminate species [13,31,33,34]. However, cationic species present in the solution also impact the precipitation of hydrates and take part in their microstructure [35]. Especially, sodium or potassium can be integrated into the main hydration products that are calcium

silicate hydrates (C-S-H) [10,13,36–38]. This substitution of calcium by alkali decreases the silicate mean chain length, but does not seem to have a significant microstructural impact on the C-S-H [36,39]. Monovalent cations also do not allow for the formation of stable and cohesive hydrates unlike divalent cation such as calcium [40–42]. This substitution could then be detrimental for the global cohesion of the cementitious matrix if the amount of alkali substitution or the alkali concentration in the solution are too high [38,43–45]. So, in order to enhance the precipitation of stable hydrates, the activating solution should present a high concentration of network modifiers cationic species with high polarization power to enhance slag dissolution while taking into account their integration into the microstructure of precipitated phases.

In a previous study, the authors showed that the amount of sodium hydroxide strongly impacts the extent and kinetics of slag hydration as well as the microstructure formed [46]. The more advanced extent of hydration and the highest mechanical properties (between 30 and 45 MPa at 28 days) being achieved with an activator content strictly superior to 5% and up to 15% of slag mass. In these conditions, the microstructure was mainly composed of calcium aluminum silicate hydrates ($Ca_vAl_wSi_xO_p(OH)_y{\cdot}z(H_2O)$, C-A-S-H) and hydrotalcite ($Mg_wAl_x(CO_3)_p(OH)_y{\cdot}z(H_2O)$) with a lower amount of calcium hemicarboaluminates ($Ca_vAl_w(CO_3)_p(OH)_y{\cdot}z(H_2O)$) and portlandite ($Ca(OH)_2$).
The main objective of this study is therefore to use alternative user-friendly activators in substitution of a part of the optimal amount of sodium hydroxide (>5 wt%) while achieving equivalent performance.

The total Na_2O content is kept constant to 5% of slag mass, which is considered to be below the optimum amount of sodium, estimated to lies between 10 and 15 wt.% of slag mass [46]. Three calcium-based activators (calcium hydroxide, calcium carbonate and calcium sulfate) and one magnesium-based activators (magnesium oxide) are used as divalent complementary activators. Calcium-based activators are chosen to enhance the ionic strength and the calcium amount of the activating solution. These parameters tend to favor the dissolution of slag [34,47] and the precipitation of cohesive hydrates [33,42–44]. Besides, increasing calcium hydroxide amount enables to maintain a pH value superior to 12.5, which enhances alkali-activation of the slag. Most of the previously cited studies about slag activation focus on mixes of sodium-based activators such as sodium silicate and sodium hydroxide. Studies with combination of calcic and sodic activators in binary or ternary activating mixes are rarer in the literature. Regarding the potential microstructure modifications, calcium sulfate is used to favor precipitation of ettringite [24,25] and calcium carbonate is used to favor precipitation of hydrotalcite [48]. Finally, magnesium oxide is used to increase the magnesium amount and to act as nucleation point to favor the precipitation of hydrotalcite [19,49–51]. Each additional activator is used individually in addition to sodium hydroxide in binary activating mixtures and in addition to sodium hydroxide and

magnesium oxide in ternary activating mixtures. The influence of complementary activators on slag activation is studied by varying the type and amount of complementary activators used whether it is in binary or ternary mixtures. The water content is also investigated. The compressive strength of the samples is measured after 28 days of hydration to assess the benefit or drawback of such activator addition. In order to understand the mechanical properties variations among the formulations and the impact of each activator addition on the hydration of slag, the microstructure and the hydrates assemblage is also studied through infrared spectroscopy, X-ray diffraction measurements, thermogravimetric and differential thermal analyses.

2. Material and Methods

2.1. Materials

The grounded blast furnace slag (GBFS) used in this study is supplied by ECOCEM France. Its composition is given in **Table 1**. The specific surface area (Blaine) is 4450 cm^2/g and the median diameter (d_{50}) is 11 µm. The good reactivity of this slag is pointed out by its basicity index, $(CaO + MgO)/SiO_2$ molar ratio, which is here superior to 1 (1.19) [52]. The physico-chemical structure of the slag has been presented in details in a previous work [46]. It is mainly composed of an amorphous silico-aluminate phase presenting an amorphous dome between 25° and 37.5° (2θ) in X-ray diffraction pattern and a large infrared absorption band between 1050 and 750 cm^{-1} associated to Si-O and Al-O vibrations. A calcium carbonate phase is also detected by the presence of specific infrared absorption bands between 1550 and 1400 cm^{-1} and at 875 cm^{-1}.

Table 1: Chemical composition (oxides weight%) of the slag.

Elements	CaO	SiO_2	Al_2O_3	MgO	SO_3	Others
Fraction (wt.%)	42.0	35.3	10.9	7.5	2.3	2.0

The different activators used are presented in **Table 2**. Sodium hydroxide is used in a liquid form. Pure pellets (purity 99.9%, Fisher Scientific) are dissolved in distilled water to prepare an alkaline activating solution. The concentration of the sodium hydroxide solution is kept constant to 4 M and the pH value is equal to 13.6. The total amount of sodium hydroxide solution used is calculated to keep a constant amount of Na_2O to 5 wt.% of slag mass. In the case of pure sodium hydroxide activation (formulation labelled as NH in **Table 3**), these conditions correspond to a free water to solid mass ratio (W/S) of 0.4. All other activators are used in the form of dry powder and directly mix with anhydrous slag prior to the addition of the sodium hydroxide solution. The additional activators are not incorporated into the

sodium activating solution to avoid any interference with the sodium hydroxide dissolution due to common ion effects [53].

Table 2: List of activators and the associated global warming potential (GWP 100a) obtained from the life cycle assessment (see section 2.2, * GWP 100a value of NaOH powder).

Activator	Used form	Label - Ecoinvent 3	GWP 100a (kg CO_2 eq / kg)
Sodium hydroxide (NaOH)	Solution	Sodium hydroxide, without water, in 50% solution state {GLO} | market for |	1.31*
Calcium hydroxide ($Ca(OH)_2$)	Powder	Lime, hydrated, packed {RER} |market for |	$8.78 \cdot 10^{-1}$
Magnesium oxide (MgO)	Powder	Magnesium oxide {GLO} |market for |	1.16
Calcium sulfate ($CaSO_4$)	Powder	Anhydrite {GLO} |market for |	$5.63 \cdot 10^{-2}$
Calcium carbonate ($CaCO_3$)	Powder	Limestone, crushed, washed {CH} |market for |	$4.97 \cdot 10^{-3}$

The total free water to dry mass ratio (W/S) was kept constant to 0.4 by adding additional water corresponding to the additional dry mass of activators used as powder. This water addition is introduced in the final mixture after the addition of the sodium hydroxide solution. The addition of water is required to avoid workability issues linked to the increase of water demand due to the use of complementary activators in a dry state. The effective concentration of sodium in the final mixture considers all the water additions (**Table 3**). The impact of an increase in water content is studied for two specific formulations, for which W/S ratio is increased to 0.5. The formulations of all the tested samples are listed in **Table 3**. The final sodium concentration is superior to 3 M for each formulation, the pH value of the interstitial solution is then considered to be superior to 13 for each sample [46].

Table 3: Formulations tested: binary and ternary mixes.

Nomenclature	Activator / Slag (wt.%)					Free water / Solid (wt.)	[Na^+] (M)
	Na_2O - (NH)	MgO - (Mg)	$Ca(OH)_2$ - (CH)	$CaSO_4$ - (CS)	$CaCO_3$ - (Cc)		
NH	5	-	-	-	-	0.4	4.0
NH_10	10	-	-	-	-		8.0
NH+Mg_2.5	5	2.5	-	-	-		3.9
NH+Mg	5	5	-	-	-		3.8
NH+Cc	5	-	-	-	5		3.8
NH+Cs	5	-	-	5	-		3.8
NH+CH	5	-	5	-	-		3.8
NH+Mg+Cc_5_5	5	5	-	-	5		3.7
NH+Mg+Cs_5_5	5	5	-	5	-		3.7
NH+Mg+CH_2.5_2.5	5	2.5	2.5	-	-		3.8
NH+Mg+CH_5_5	5	5	5	-	-		3.7
$NH_{/0.5}$	5	-	-	-	-	0.5	3.2
NH+Mg_$5_{/0.5}$	5	5	-	-	-		3.1

The samples were cast in cylindrical molds (diameter: 2 cm; height: 4 cm) after 1 min of manual mixing. The molds were kept closed to avoid water evaporation or drying. The samples were demolded after 24 hours at ambient conditions (20-25°C / 30-40% RH) and individually sealed for endogenous curing. All testing methods were performed after 28 days of curing.

2.2. Characterization methods

The uniaxial compressive strength of the samples was tested using a Zwick universal testing machine equipped with a 100 kN load cell (class 0.5). The crosshead speed was set to 0.3 mm/min. Three different samples are tested at 28 days for each formulation.

Infrared spectroscopy measurements (FTIR) were performed using a TermoFisher Scientific IS50 device in the Attenuated Total Reflection (ATR) mode. The spectra were acquired from 4000 to 400 cm^{-1}, with a spectral resolution of 4 (digital step of 0.5 cm^{-1}) and averaged on 32 scans. Data were analyzed using Omnic Series software with a baseline correction treatment. All spectra were normalized with respect to the water absorbance band at 1640 cm^{-1}.

Thermogravimetric (TGA) and differential thermal analysis (DTA) were performed on a Labsys Evo device (Setaram, France) up to 1100°C with a heating rate of 10°C/min and under dry air with a fixed flow of 20 mL/min. Alumina crucible were used with a constant sample mass of 50.0 ± 0.5 mg. Baseline corrections were operated with a blank measurement realized on an empty alumina crucible.

X-ray diffraction patterns were acquired with a D8 Advance diffractometer (Brucker, Germany) using CuKα radiation (λKα = 0.154186 nm), an acquisition step of 0.02° (2θ) between 5° and 65° (2θ), and a dwell time of 2.5 s. Data were analyzed using EVA software with background and $K\alpha_2$ corrections. Identification of crystalline phases was made by comparison with PDF standards (Powder Diffraction Files) from ICDD (International Centre for Diffraction Data).

Scanning electron microscopy (SEM) observations were performed on a Vega 3 SEM (Tescan, Czech Republic) equipped with a tungsten filament. Observations were made on gold coated samples in back scattering electron (BSE) mode, with an acceleration voltage of 5 kV and a working distance of 5 mm.

The environmental impact of the activator mixes are evaluated through a cradle-to-gate assessment [54]. For comparison purpose, only the impact of activators needed for the activation of 1 kg of slag were considered and the environmental impact of slag or water content were not taken into account. The life cycle inventory (LCI) datasets are obtained from the Ecoinvent 3 database [55] (**Table 2**). The environmental impacts of the activators mainly depend on the industrial processes from which they are produced [12] and on the energy mix of the country of production [56]. This is especially true for sodium hydroxide production which mainly requires electricity. No specific further transportation distance was considered, since this approach is only relevant for projects with a specific location. The life cycle impact assessment (LCIA) method used was the CML-IA baseline method (version 3.06) [57], which indicators are given in **Table 4.** The total impact of each formulation, for each indicator *i*, is then given by (1):

$$Total\ Impact_i = \sum_{j=1}^{n} m_j \cdot Imp_j \quad (1)$$

Where m_j is the weight content of activator *j* and Imp_j is the impact factor for 1 kg of activator *j* produced.

The analyses were conducted on SimaPro v9.1.1 software.

Table 4: Environmental indicators and units for the CML-IA baseline (v3.06) method.

Environmental indicators	Unit
Abiotic Depletion	kg Sb eq
Abiotic Depletion (fossil fuels)	MJ
Global Warming Potential (GWP 100a)	kg CO_2 eq
Ozone Layer Depletion	kg CFC-11 eq
Human Toxicity	kg 1,4-DB eq
Fresh Water Aquatic Ecotoxicity	kg 1,4-DB eq
Marine Aquatic Ecotoxicity	kg 1,4-DB eq
Terrestrial Ecotoxicity	kg 1,4-DB eq
Photochemical Oxidation	kg C_2H_4 eq
Acidification	kg SO_2 eq
Eutrophication	kg $(PO_4)^{3-}$ eq

3. Results

3.1. Binary mixtures

The compressive strength along with the total sodium concentration obtained for all binary mixtures are presented in Fig. 1. A compressive strength of 26.4 MPa with 5 wt.% of Na2O is considered as a reference value (dashed line). The addition of 2.5 wt.% of MgO shows no significant modification of the compressive strength (+ 3%), while a further addition up to 5 wt.% is detrimental (- 9%). The addition of water is detrimental for compressive strength in any cases: - 31% and – 41% for NaOH and NaOH-MgO activated slag respectively. The latter combines the detrimental effects of a too important addition of MgO and of addition of water. The negative effect of water addition is well documented for hydrated materials such as cements [58]. In the case of alkali-activated materials an increase in water content also implies a decrease of activators concentration (Fig. 1), which has an important impact both on hydration reaction and on compressive strength [46].

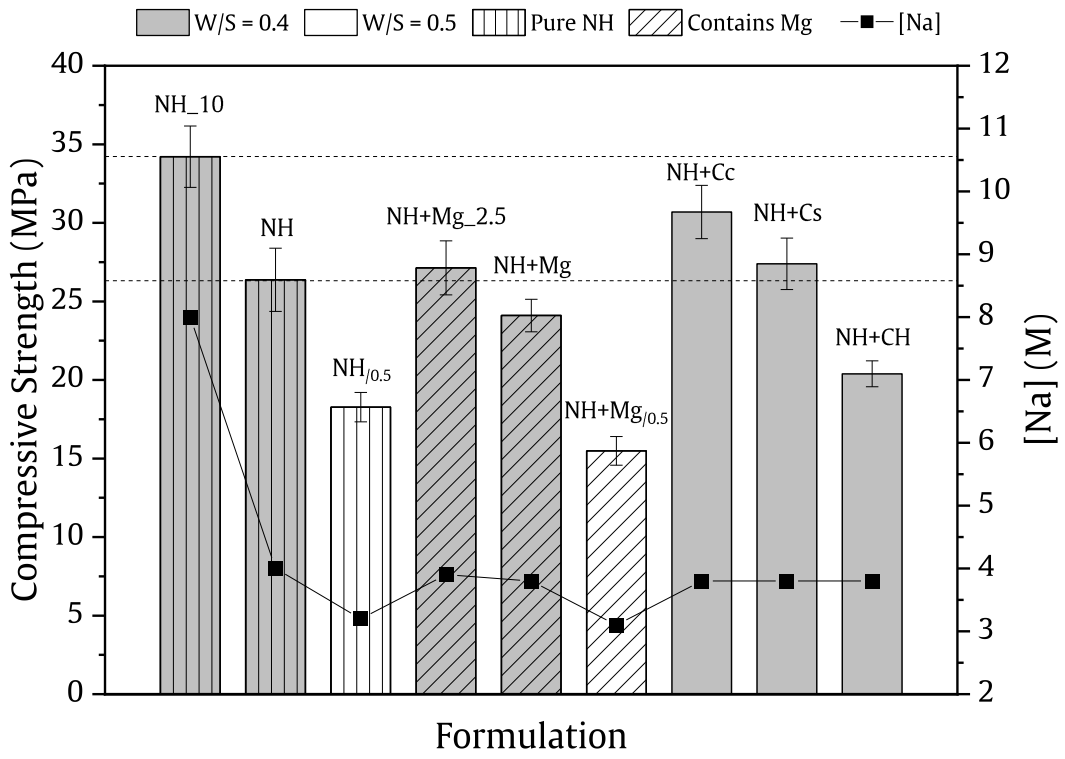

Fig. 1. Compressive strength at 28 days and effective sodium concentration (square symbols) of samples activated with pure sodium hydroxide and with binary mixtures. Samples activated with a water ratio of 0.5 are white filled. Straight hatching is for samples activated with pure sodium hydroxide solution and diagonal hatching is for samples activated with NaOH and MgO. The dashed lines refer to the compressive strength of the NH and NH_10 samples (26.4 and 34.2 MPa respectively).

Samples activated with a complementary calcic activator (Cc, Cs or CH) show a different mechanical behavior, although the total sodium concentration is kept constant. Hence, the addition of 5 wt.% of calcium carbonate leads to a significant increase (+ 16%) and presents the highest compressive strength of all formulations tested with binary mixtures (30.7 MPa), while the use of 5 wt.% of calcium sulfate presents an increase of 4% and the use of 5 wt.% of calcium hydroxide shows an important decrease of 23% as compared to the mechanical properties of NH sample.

The influence of the activator mix on hydrated microstructures after 28 days of hydration has been studied. **Fig. 2** presents the infrared spectra obtained for the samples activated with binary mixtures and the NH formulation. The microstructure obtained with the NH_10 formulation has been discussed and compared to the one obtained with NH formulation in a previous work [46]. All the samples present a spectrum with a main band at 932 cm^{-1} completed by bands at 812 and 650 cm^{-1} (**Fig. 2**) which are all

associated to Si-O and Al-O vibrations in C-A-S-H [38,59–61]. A slight shoulder at 890 cm^{-1}, more or less well defined depending on the samples, is associated to the formation of hydrotalcite [46] and especially to Al-O bonds [61]. Finally, the bands at 710 and 1385 cm^{-1} are associated to hydrated carbonates [62–64], showing a significant dissolution and hydration of initial anhydrous slag [46]. Then, no substantial chemical modification of the microstructure formed whatever the complementary activator used is noted. The band at 1640 cm^{-1}, associated to free water, and the broad band between 2800 and 3800 cm^{-1} associated to –OH vibrations are present in all spectra.

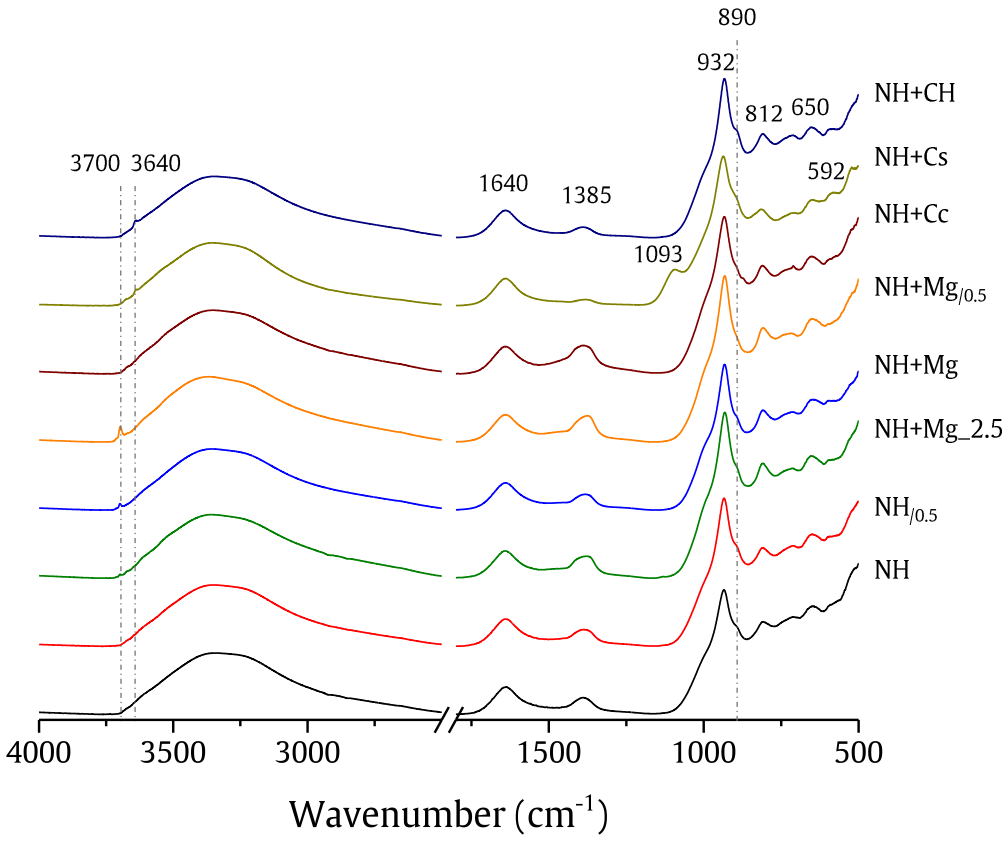

Fig. 2. FTIR spectra between 500 and 4000 cm^{-1} of samples activated with pure sodium hydroxide and with binary mixtures after 28 days of curing.

The samples prepared with an addition of MgO present another band at 3700 cm^{-1} (**Fig. 2**) associated to Mg-OH bond stretching vibrations [65–67], thus indicating MgO dissolution and/or its integration in hydrated phases. The intensity of this band increases with MgO content and is maximal for the sample containing 5 wt.% of MgO and additional water ($NH+Mg_{/0.5}$). The hydrated carbonate band at 1385 cm^{-1} is also slightly increased for this sample, indicating a more pronounced carbonatation. The bands

associated to carbonates group are maximal for the sample containing an additional amount of calcium carbonate (NH+Cc). No band shifts are observed for the hydrated carbonate bands, indicating the formation of similar carbonated groups than in the other formulations. With the use of Cs, the carbonatation is especially low. Supplementary bands are observed for this particular sample at 592 and 1093 cm^{-1}, associated to out-of-plane bending vibrations (ν_4) and asymmetric stretching vibrations (ν_3) of SO_4^{2-} groups respectively [60,68,69]. The microstructure and the nature of the precipitated hydrates are then different than in the other formulations. Finally, a small band at 3640 cm^{-1} is associated to the stretching vibrations of OH groups in portlandite ($Ca(OH)_2$) [38,65,66,70]. The band associated to portlandite is even more visible in the sample activated with calcium hydroxide CH, suggesting that a non-negligible amount of this activator has not reacted with the slag. As for the sulfate-activated sample, the carbonate band at 1385 cm^{-1} is less noticeable than for the other formulations.

X-ray diffraction patterns of binary formulations are presented in **Fig. 3**. No peaks associated to the initial calcium sulfate nor to magnesium oxide are detected, suggesting a total dissolution of these anhydrous activators. The main hydrated phase formed by all the activator mixtures is a C-A-S-H gel. The microstructure is completed by various amounts of hydrotalcite (Ht) and calcium hemicarboaluminates (CHc) depending on the activating mix. In particular, the addition of water in pure sodium-activated sample does not modify the nature of the crystalline phases formed. When comparing the magnesium-activated samples with pure sodium-activated ones, it appears that magnesium addition broadly favors hydrotalcite over hemicarboaluminate precipitation.
This tendency seems to depend more on the magnesium concentration than on the total magnesium amount in the system. Indeed, the X-ray pattern of the sample with 5 wt.% of MgO and W/S of 0.5, and thus with a lower magnesium concentration, is closer to the one with 2.5 wt.% MgO and W/S of 0.4 than the one with 5 wt.% of MgO and W/S of 0.4. Especially, the highest magnesium concentration in the sample NH+Mg promotes hydrotalcite and calcite (C) formation while it hinders CHc precipitation. Brucite ($Mg(OH)_2$) is not observable, suggesting that the Mg-OH bounds observed in infrared spectra (**Fig. 2**) are related to magnesium groups well-integrated in hydrated structures such as hydrotalcite.

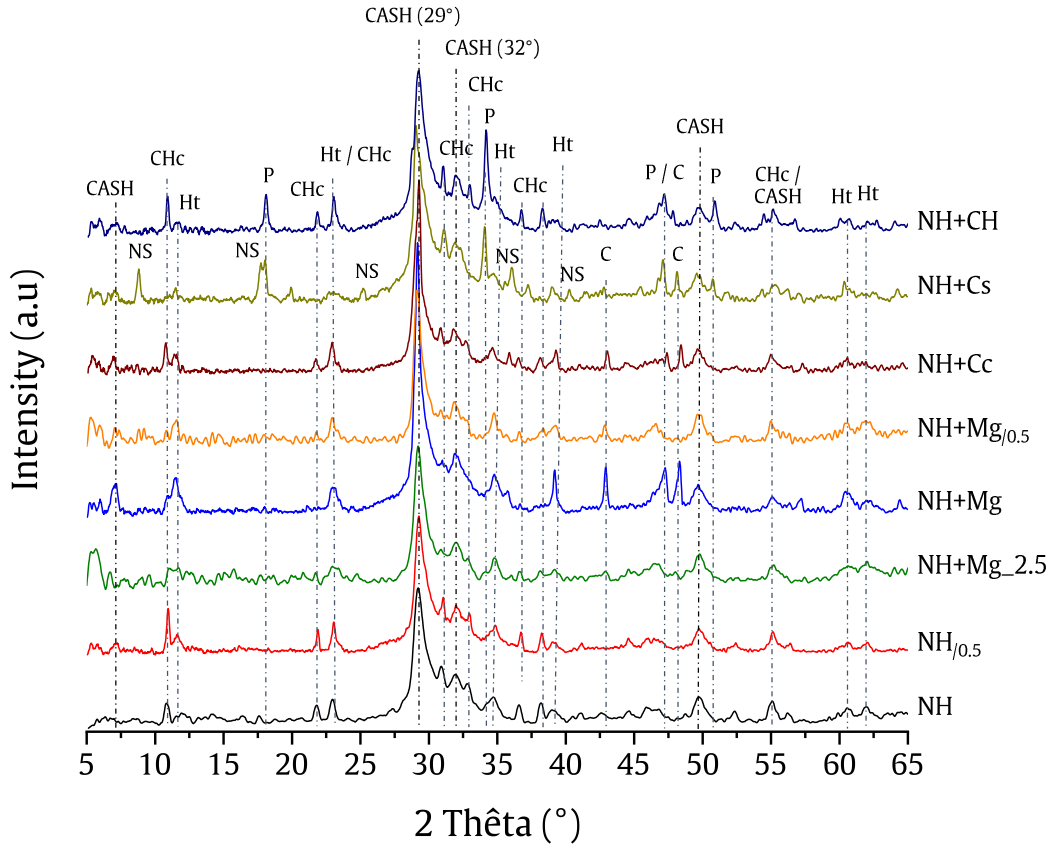

Fig. 3. X-ray diffraction patterns of the samples activated with binary mixtures and of the pure sodium-activated sample at 28 days. C-A-S-H: PDF #00-034-0002, CHc: calcium hemicarboaluminate - PDF#00-041-0221, Ht: hydrotalcite - PDF#00-014-0191, P: portlandite - PDF#00-044-1481, NS: sodium calcium aluminum sulfate hydrate - PDF#00-044-0272 and C: calcite - PDF#01-081-2027.

In the sample activated with an addition of calcium carbonate, a larger amount of calcite is observable but the diffractogram is very similar than the one of pure sodium-activated samples. The presence of calcium sulfate leads to the precipitation of a sodium calcium aluminum sulfate hydrate (NS) and portlandite (P), confirming the observations from infrared spectroscopy (**Fig. 2**). The precipitation of hydrotalcite, but above all of hemicarboaluminate, is hindered while a slight amount of calcite is observable. Finally, the presence of calcium hydroxide in the activating mixture promotes hemicarboaluminate precipitation over hydrotalcite and the excess is present in the form of portlandite.

The relative mass fractions of hydrated and carbonated phases have been evaluated through thermogravimetric analyses. The temperature ranges associated to each phase are presented in **Table 5**.

Table 5: Temperature ranges of the mass losses associated to each identified phase (from XRD analysis). CHc: calcium hemicarboaluminate, Ht: hydrotalcite, P: portlandite, NS: sodium calcium aluminum sulfate hydrate and C: calcite.

Phase	Free Water	C-A-S-H	CHc	NS	Ht	P	Carbonates
Temperature Range (°C)	0 - 100	100 - 170	170 - 280	180 – 300	280 - 415	415 - 500	650 - 900
References	[71,72]	[11,24,72–74]	[26,75]	[75]	[11,24,50,71,73,76–78]	[61,71,73,79,80]	[25,72,81]

The mass loss associated to each hydrated phase (**Table 6**) and the corresponding relative mass fraction (mass loss / total mass loss) labelled in **Fig. 4** correspond to the mass loss measured in the ranges mentioned in **Table 5**. It should be noted that the relative mass fractions are only semi-quantitative and should be used for comparison purposes between the different samples and not for a precise quantification of the phases fractions, and this for two reasons. The first one is that the effective mass losses of different phases overlap in a broad range of temperatures, especially between 100 and around 180°C. In this range, water molecules from different phases, more or less bounded into hydrated structures, can be extracted. It could lead to an overestimation of C-A-S-H and CHc contents and to an underestimation of the content of other hydrated phases. The second reason is that for an accurate quantitative estimation of one phase, the exact chemical formula and especially the water stoichiometry should be precisely known to link the water mass loss to the corresponding mass of hydrates. This is not the case in complexes systems such as alkali-activated slag binders. Nevertheless, the calculation presented are consistent with the previous observations made from the other characterization techniques.

Table 6: Total mass loss up to 900°C and mass loss associated to each identified hydrated phase for samples activated with pure sodium hydroxide and with binary mixtures after 28 days of curing.

Formulation	Total mass loss (%)	Mass loss related to each phase (%)						
		Free water	C-A-S-H	CHc	Ns	Ht	P	Carbonates
NH	22.84	4.57	12.21	3.60	-	1.84	0.40	0.22
NH$_{/0.5}$	25.92	5.28	15.47	3.08	-	1.63	0.40	0.06
NH+Mg_2.5	25.93	4.75	14.41	3.87	-	2.28	0.42	0.20
NH+Mg	23.97	6.03	11.97	3.04	-	2.47	0.38	0.08
NH+Mg$_{/0.5}$	27.36	6.42	14.40	3.39	-	2.48	0.42	0.25
NH+Cc	21.66	4.24	11.05	3.20	-	1.60	0.31	1.26
NH+Cs	22.12	5.35	11.60	-	2.84	1.39	0.85	0.09
NH+CH	23.64	6.02	10.86	3.69	-	1.73	1.26	0.08

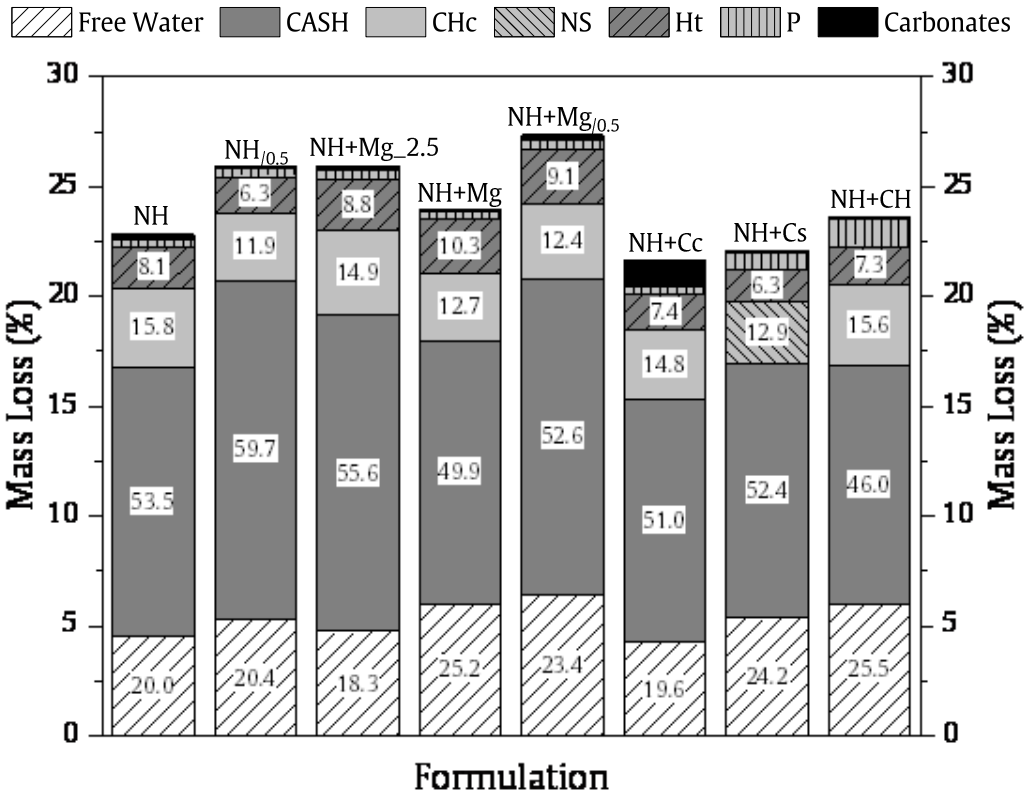

Fig. 4: Semi-quantitative phase distribution of the total mass loss of samples activated with pure sodium hydroxide solution and with binary mixtures at 28 days. The labelled numbers correspond to the percentage of the total mass loss associated to the main phases. CHc: calcium hemicarboaluminate, Ht: hydrotalcite, P: portlandite, NS: sodium calcium aluminum sulfate hydrate and C: calcite.

The samples presenting the most important proportion of free water are those with an addition of calcium hydroxide, calcium sulfate and high amount of magnesium oxide (5 wt.%). The addition of water does not significantly increase the amount of free water for both formulations tested (**Table 6**). The total mass loss and the proportion of CASH are increased and the proportion of CHc and hydrotalcite are decreased as compared to the corresponding formulation with a water ratio of 0.4 (**Fig. 4**). The thermogravimetric analyses confirm the fact that CHc precipitation is also hindered by an addition of magnesium oxide, especially at high magnesium content, and by an addition of calcium sulfate. Besides, the addition of 5 wt.% of magnesium oxide slightly increases the precipitation of hydrotalcite. Conversely, in the case of a calcium hydroxide addition, the precipitation of CHc is favored over hydrotalcite one. The amount of portlandite formed is increased with an addition of calcium sulfate and is the highest with an addition of calcium hydroxide.

Fig. 5 shows the SEM observations of samples activated with sodium hydroxide and binary mixtures. The sample activated with sodium hydroxide presents a dense structure of C-A-S-H gel with a honeycomb-like morphology. The sample containing 2.5 wt.% of MgO presents a similar structure with a clearly visible proportion of CHc hydrates incorporated in the C-A-S-H matrix. However, when the MgO content is increased up to 5 wt.%, large and poorly hydrated slag grains are observable. The anhydrous or poorly hydrated slag grains are easily identifiable by their smooth and angular surfaces. These grains are surrounded by a matrix of C-A-S-H and hydrotalcite gel. Slag grains are also observable with the sample activated by calcium hydroxide (NH+CH). This latter presents large platelets of portlandite included in the C-A-S-H and hydrotalcite matrix. The calcium carbonate and calcium sulfate samples present a dense C-A-S-H gel structure containing respectively CHc and NS hydrates. It is worth noting that the NS hydrates seem to have precipitated in very specific sites which could correspond to the presence of initially anhydrous calcium sulfate particles. These observations confirm the nature of hydrated phases as identified by FTIR (**Fig. 2**) and XRD (**Fig. 3**) analyses.

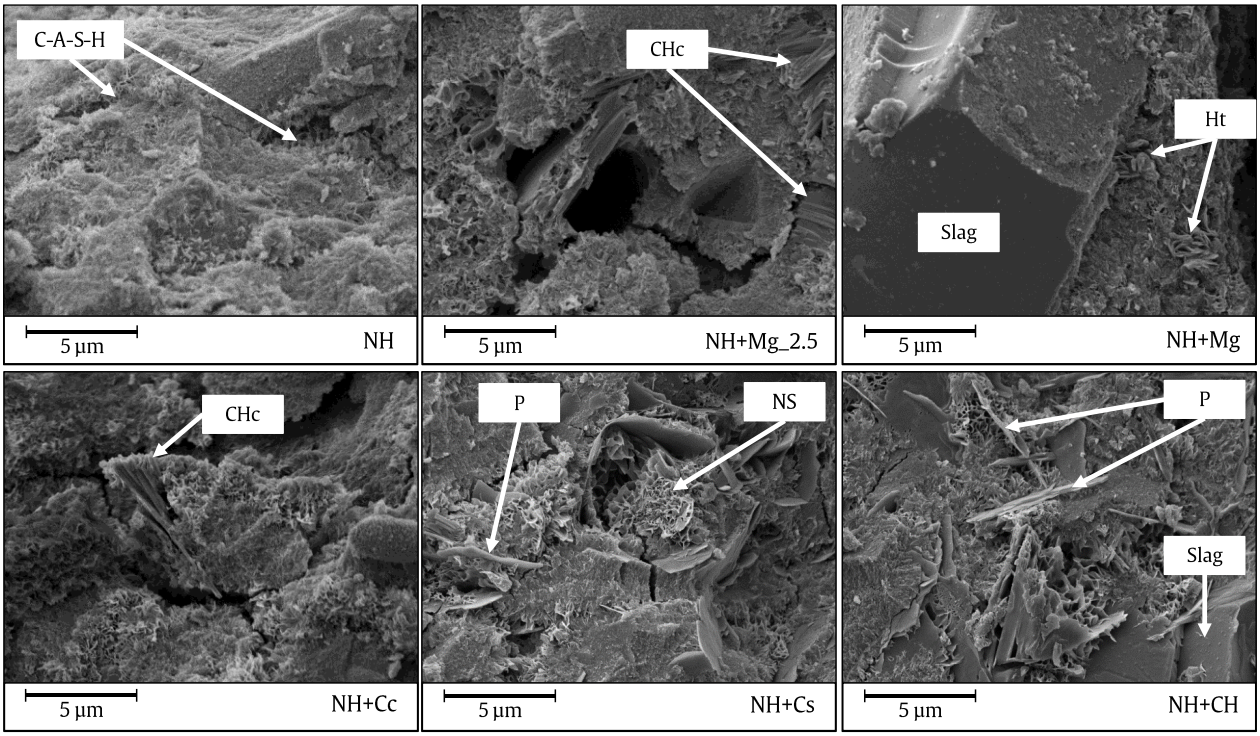

Fig. 5: SEM images at 28 days of samples activated with pure sodium hydroxide and with binary mixtures (see label on the bottom right of each image). CHc: calcium hemicarboaluminate, Ht: hydrotalcite, P: portlandite and NS: sodium calcium aluminum sulfate hydrate.

Concerning the samples activated with an addition of water (**Fig. 6**), the observed C-A-S-H gel structure are less dense than for the other samples. It is mainly due to the presence of large anhydrous slag grains

in the structure identifiable in the two concerned samples. In addition to the main C-A-S-H gel, only traces of hydrotalcite or CHc hydrates are noted.

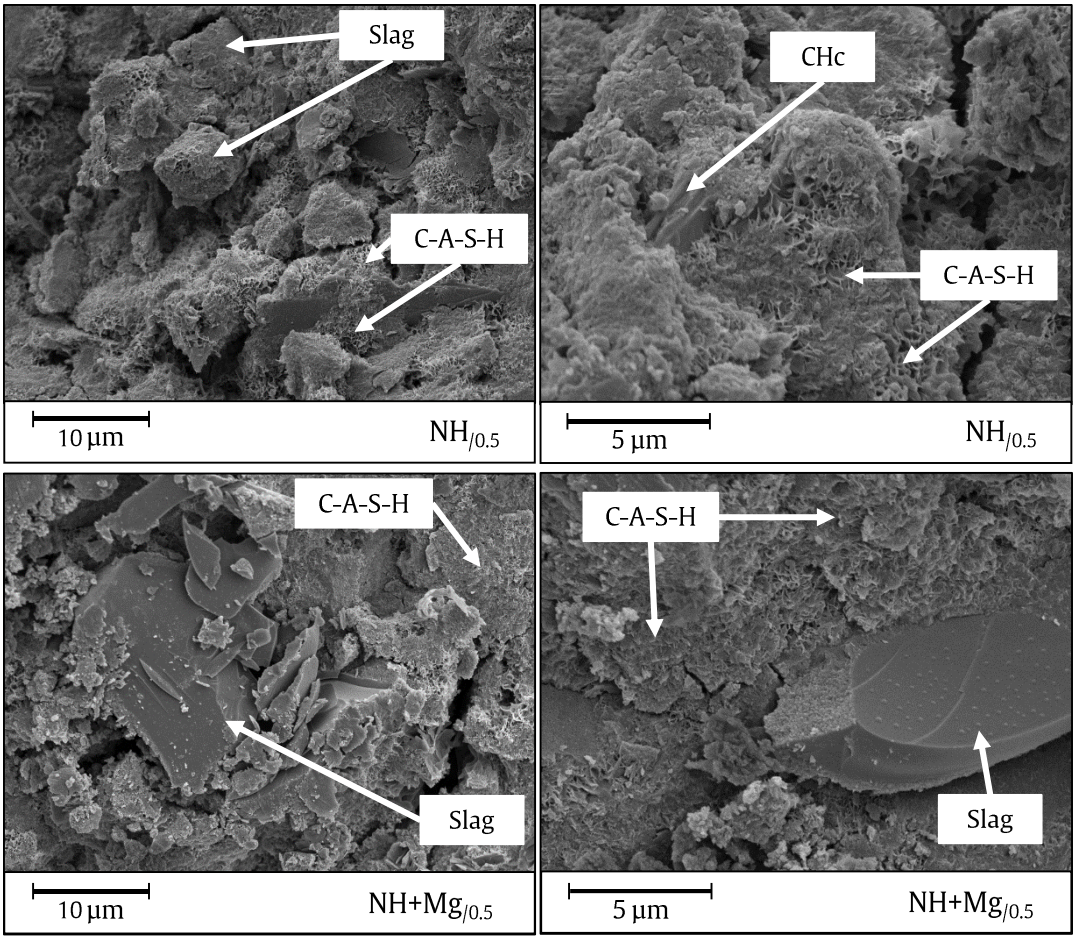

Fig. 6: SEM images at 28 days of samples with water addition. CHc: calcium hemicarboaluminate.

3.2. Ternary mixtures

The mechanical properties of the samples activated with ternary mixtures are presented in **Fig. 7**. As for the binary mixtures, the pure sodium-activated sample is taken as a reference (compressive strength after 28 days of 26.4 MPa) and the total sodium concentration of the activating mix is plotted with dark squares for each sample.

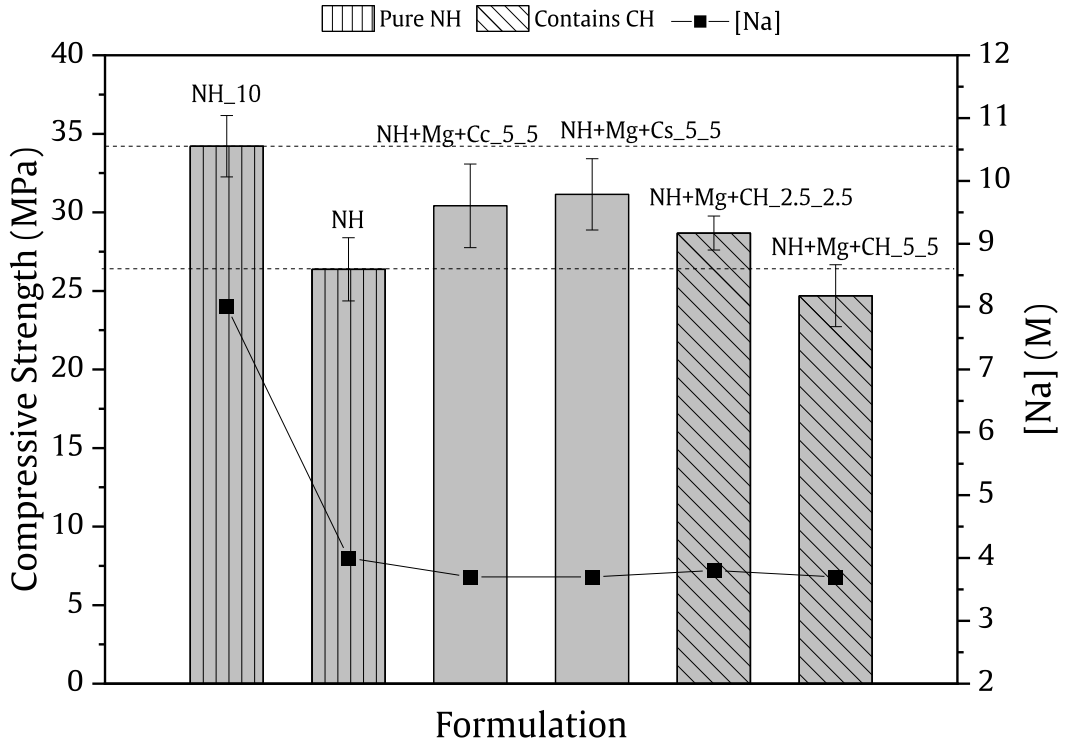

Fig. 7. Compressive strength and effective sodium concentration (square symbols) of samples activated with pure sodium hydroxide and ternary mixtures obtained after 28 days of curing. Straight hatching is for samples activated with pure sodium hydroxide solution and reverse diagonal hatching is for samples activated with an addition of calcium hydroxide. The dashed lines refer to the compressive strength of the NH and NH_10 samples (26.4 and 34.2 MPa respectively).

The samples activated with an addition of both magnesium oxide and calcium carbonate (NH+Mg+Cc_5_5) or calcium sulfate (NH+Mg+Cs_5_5) present a higher compressive strength than the reference despite a lower total sodium concentration in the activating mix (-7.5%). The compressive strength increase is about 15% and 18% for calcium carbonate and calcium sulfate respectively. The sample activated with an addition of calcium hydroxide presents a slight increase of the compressive strength (+9%) when the amount of magnesium and calcium hydroxide are kept to a low level (2.5 wt.%). However, these additions become detrimental for mechanical properties when their amount is raised to 5 wt.%.

The infrared spectra of the samples activated with ternary mixture present similar shapes since the main observable bands of absorption are those associated to C-A-S-H (650, 812 and 932 cm^{-1}), hydrated

carbonates (1385 cm^{-1}) and free water (1640 cm^{-1}) (**Fig. 8**). The shoulder at 890 cm^{-1} is associated to the presence of hydrotalcite. Nonetheless, some differences between samples can be pointed out. Considering the sample activated with calcium sulfate, the bands associated to C-A-S-H are less sharps than for the other formulations and the two bands associated to sulfate groups at 592 and 1093 cm^{-1} are present, like in the binary mixture containing calcium sulfate (**Fig. 2**). Besides, a band at 1473 cm^{-1} is also present for this sample and, to a lesser extent, for the one containing calcium carbonate. This band is associated to Ca-CO_3 vibrations [68,70,82,83] and is not observable in other samples, indicating a modification of the chemical environment of a part of carbonate groups.

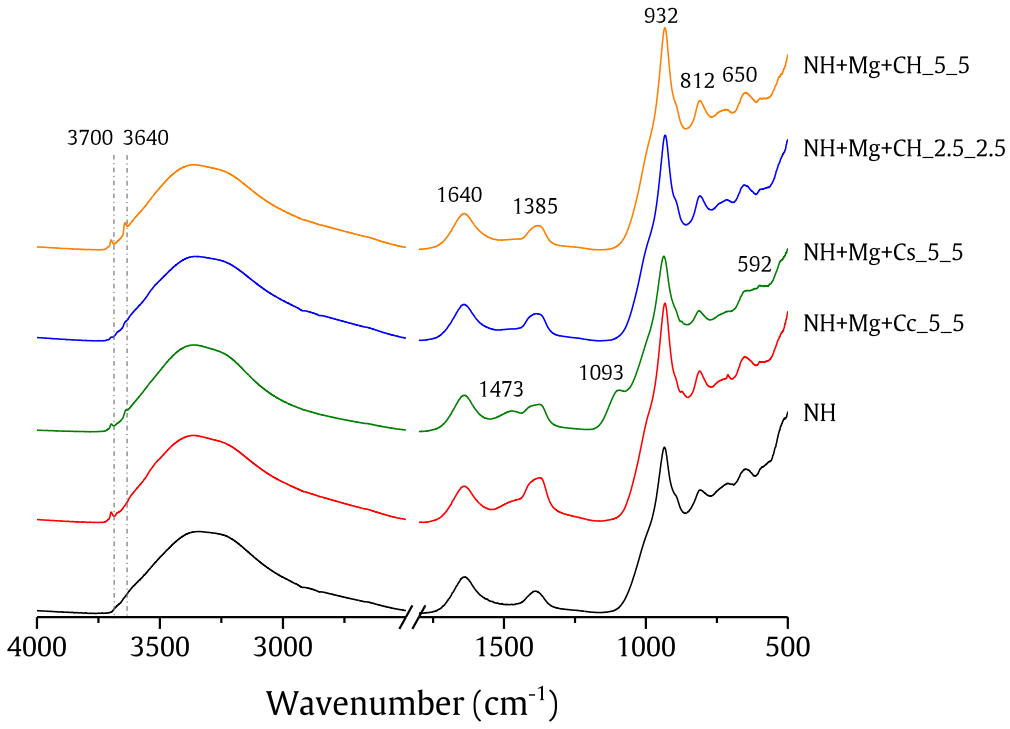

Fig. 8. FTIR spectra between 500 and 4000 cm^{-1} of samples activated with pure sodium hydroxide and with ternary mixtures obtained after 28 days of curing.

As for binary mixtures, the samples containing a magnesium amount superior to 2.5 wt.% present a band at 3700 cm^{-1} related to Mg-OH stretching vibrations (**Fig. 8**). Finally, the Ca-OH vibration band at 3640 cm^{-1} is observable for the sample containing calcium sulfate and for the sample with the highest amount of calcium hydroxide (5 wt.%).

This observation is confirmed by XRD results, since portlandite is identifiable and well defined for these two samples (NH+Mg+Cs_5_5 and NH+Mg+CH_5_5 in **Fig. 9**). As well as for the binary mixtures, the main phases identifiable by XRD for the ternary mixtures are C-A-S-H, CHc and hydrotalcite (Ht) (**Fig. 9**). The main differences with the results obtained for the binary mixtures and for the pure sodium-activated sample lie in the fact that all the samples activated with ternary mixtures contains some calcite (C) and low amount of CHc. Especially, calcite is well crystallized in the samples containing calcium sulfate and calcium carbonate, confirming the infrared observations (**Fig. 8**). The same sulfate-based hydrate detected in the binary mixture containing calcium sulfate is observable in the presence of magnesium oxide and calcium sulfate. No peaks associated to the initial calcium sulfate nor to magnesium oxide are detected.

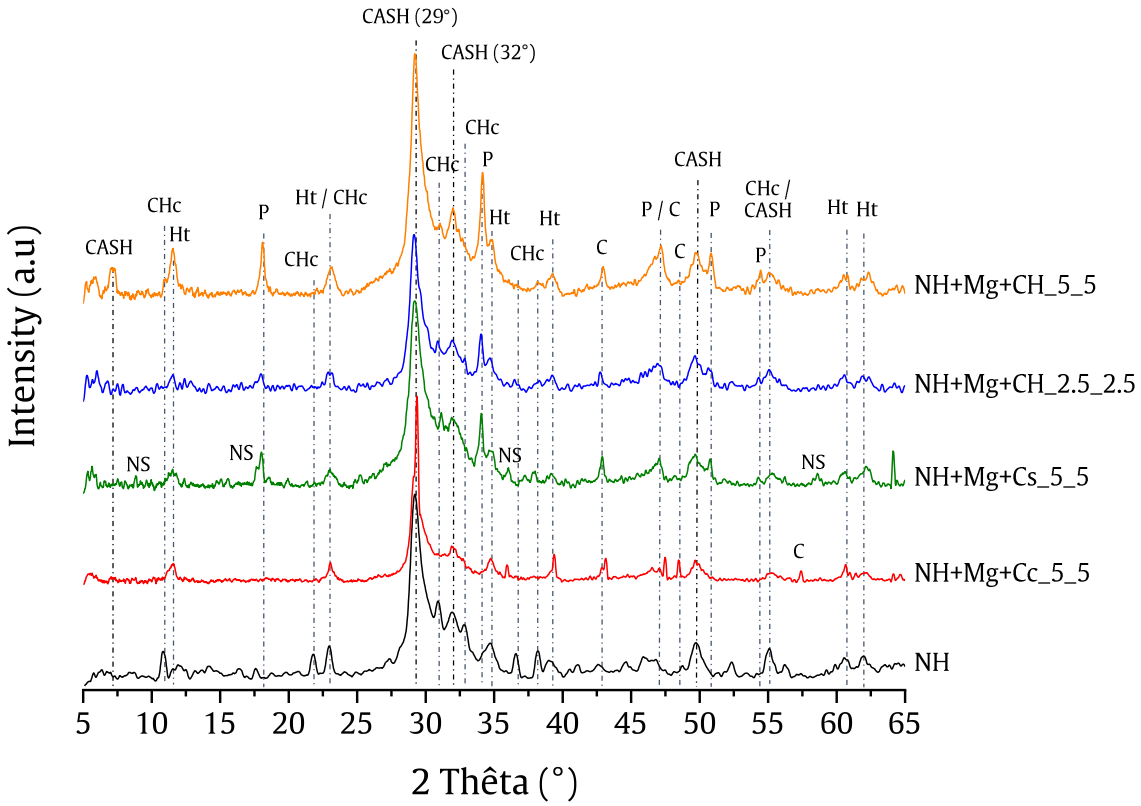

Fig. 9. X-ray diffraction patterns of the samples activated with ternary mixtures and of the pure sodium-activated sample at 28 days. CHc: calcium hemicarboaluminate, Ht: hydrotalcite, P: portlandite, NS: sodium calcium aluminum sulfate hydrate and C: calcite.

The thermogravimetric analyses of the samples activated with ternary mixtures are presented in **Table 7** and **Fig. 10** with the pure sodium-activated sample for comparison.

Table 7: Total mass loss up to 900°C and mass loss associated to each identified phase (from XRD analysis) for samples activated with pure sodium hydroxide and with ternary mixtures after 28 days of curing.

Formulation	Total mass loss (%)	Mass loss related to each phase (%)						
		Free water	C-A-S-H	CHc	Ns	Ht	P	Carbonates
NH	22.84	4.57	12.21	3.60	-	1.84	0.40	0.22
NH+Mg+Cc_5_5	24.10	4.72	14.46	-	-	3.11	0.37	1.44
NH+Mg+Cs_5_5	22.87	5.02	13.09	-	2.34	1.79	0.38	0.25
NH+Mg+CH_2.5_2.5	24.72	5.10	12.25	3.63	-	2.34	0.82	0.58
NH+Mg+CH_5_5	22.76	5.43	10.92	2.89	-	2.39	0.97	0.16

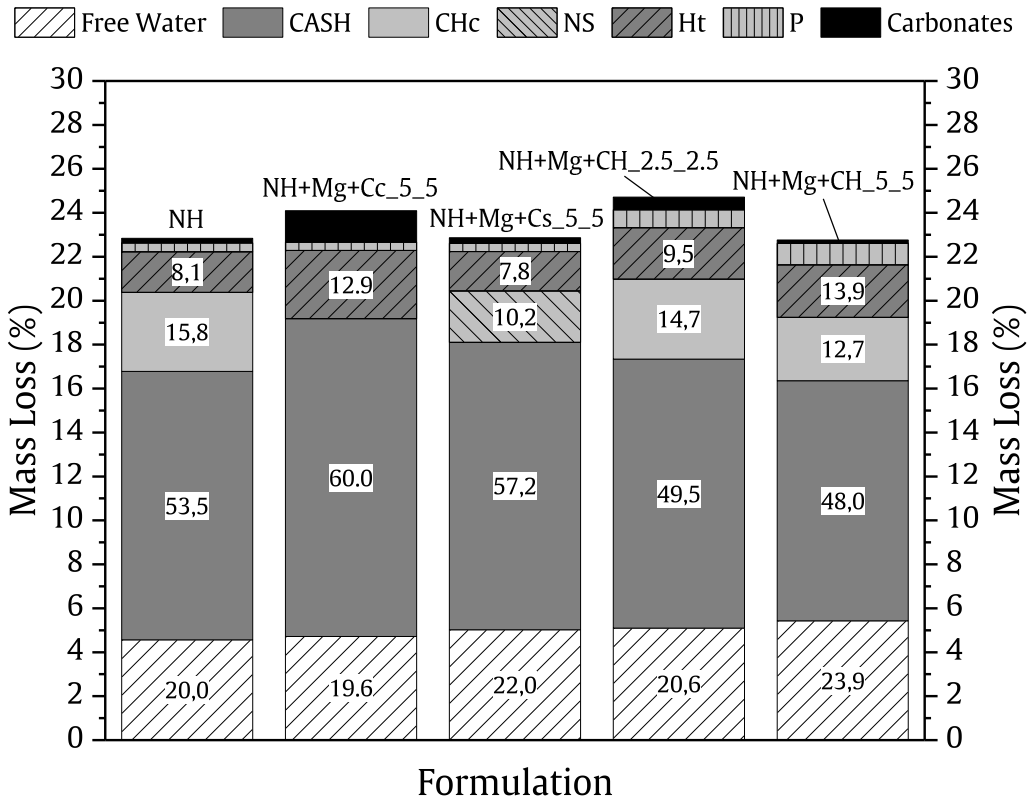

Fig. 10. Semi-quantitative phase distribution of the total mass loss of samples activated with pure sodium hydroxide solution and with ternary mixtures at 28 days. The labelled numbers correspond to the percentage of the total mass loss associated to the main phases. CHc: calcium hemicarboaluminate, Ht: hydrotalcite, P: portlandite, NS: sodium calcium aluminum sulfate hydrate and C: calcite.

The total amount of free water is slightly higher for the samples containing calcium sulfate and 5 wt.% of calcium hydroxide. The obtained mass losses are similar than the ones measured for the samples activated with binary mixtures (**Fig. 4**). C-A-S-H amount is lower for the samples containing calcium hydroxide. The addition of magnesium oxide in combination with calcic activators promotes the precipitation of hydrotalcite over CHc in all the samples. The lower proportion of hydrotalcite for the sample with calcium sulfate can be explained by the presence of the sodium calcium aluminum sulfate hydrate.

The SEM observations of the samples activated with ternary mixtures are shown in (**Fig. 11**). They all present highly dense C-A-S-H gel structure combined with varying amount of complementary phases. Few carbonates are observable in the sample activated with calcium carbonate (NH+Mg+Cc_5_5) along with well-integrated hydrotalcite phases. The honeycomb-like structure of the C-A-S-H is clearly observable in the calcium sulfate-containing sample (NH+Mg+Cs_5_5) as well as portlandite and NS hydrates. The impact of magnesium oxide and calcium hydroxide contents on the microstructure are

also visible using SEM observations. Although the two samples present a dense C-A-S-H gel matrix, the sample with low complementary activators contents (NH+Mg+CH_2.5_2.5) present a relatively high amount of well crystallized CHc hydrates. However, when the activators contents increase (NH+Mg+CH_5_5), the amount of calcite and portlandite precipitation is also increased. Besides, poorly hydrated slag grains are noted in this sample.

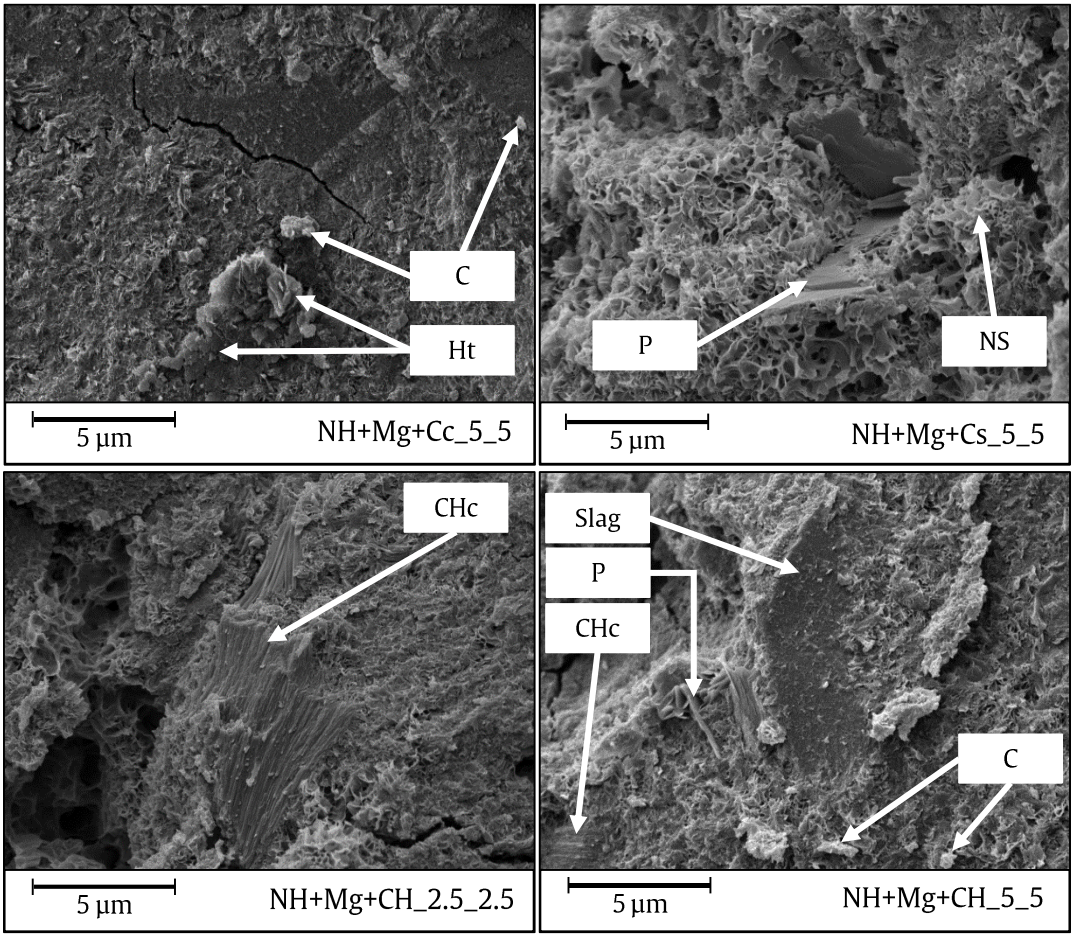

Fig. 11: SEM images at 28 days of samples activated with pure sodium hydroxide and with ternary mixtures. CHc: calcium hemicarboaluminate, Ht: hydrotalcite, P: portlandite, NS: sodium calcium aluminum sulfate hydrate and C: calcite.

4. Discussion

The addition of complementary activators impacts both the compressive strength (**Fig. 1** and **Fig. 7**) and the nature and relative proportions of hydrates formed during slag hydration (**Fig. 4** and **Fig. 10**). However, whatever the chemical nature and the amount of complementary activators studied in this

work, the overall microstructure of the hydrates assemblage is not significantly modified for binary (**Fig. 2**) or ternary mixtures (**Fig. 8**). The main hydrated phases formed are a relatively dense C-A-S-H gel, with very similar chemicophysical microstructure, containing various amount of hydrotalcite and hemicarboaluminate hydrates (**Fig. 3** and **Fig. 9**). This result stands even for ternary mixtures for which the total mass of complementary activators is higher than the one of sodium hydroxide. This emphasizes that, under these conditions, slag hydration is mainly conducted by the sodium concentration of the activating solution.

Impact of higher water content

Indeed, the addition of water up to a fraction of 0.5 to the dry mass leads to a decrease of 20% in sodium concentration (**Table 3**) which is clearly detrimental for the mechanical performances (**Fig. 1**). Nonetheless, the total amount or the relative proportion of free water observed in the concerned samples is not significantly higher than the samples with a 0.4 water ratio (**Fig. 4**). Then, the decrease in compressive strength is not only associated to an excess of water but to the decrease in activators concentration. The reduction of the activators concentration leads to a lower extent of hydration which is clearly visible on SEM observations by the presence of poorly hydrated slag grains at 28 days (**Fig. 6**). The reduction of the extent of hydration is also associated to a decrease in hemicarbonate and hydrotalcite fraction in the hydrates assemblage, as already showed in [46]. Thus, the reduction of sodium concentration in the activating solution hinders the activation process, leading to a lower proportion of hemicarbonate and hydrotalcite and to lower mechanical properties. It is worth noting that the pH value is estimated sufficiently high in all the samples, which suggests that the sodium concentration is a critical parameter over pH value for slag activation. This result is consistent with other studies where a reduction of the Na_2O content, in the range of 3-6% of slag mass, led to a significant decrease of compressive strength at 28 days [6,8]. Besides, the authors have shown in a previous work [46] that a concentration of 4 M is in the lower range for a satisfactory activation of slag, thus a further reduction is expected to be critical for slag hydration.

The use of complementary activators promotes or hinders precipitation of specific phases depending on their amount and on their chemical nature. This is one of the reasons why a similar sodium concentration in the activating solution with different complementary activators, for binary (3.8 M) or ternary mixtures (3.7 M), does not lead to similar compressive strengths (**Fig. 1** and **Fig. 7**).

Effect of calcic activators addition

Considering the different molar mass of these activators, the molar addition of calcium per gram of slag is as follows for an activator addition of 5 wt.%: Cs = 0.367 mmol/g ; Cc = 0.499 mmol/g ; CH = 0.675 mmol/g. Nonetheless, the concentration of effectively active calcium cations dissolved in the solution, which could participate to slag dissolution and hydrates precipitation, depends on the solubility of each activator in the highly alkaline medium of the activating solution (pH = 13.6). In addition to the high pH value of this solution, the high concentration in alkali (> 3M) plays an important role in the solubility behavior of this compounds. The solubility of CH decreases significantly with increasing sodium concentration in solution [53]. However, the solubility of Cs increases with pH value above 11.0 [84] and the one of Cc increases significantly with alkali concentration [85]. The good solubility of these activators is shown by the fact that no traces of initial Cc or Cs were found in the samples (**Fig. 3** and **Fig. 9**). So that, the activating potential of each activator appears as not directly related to the total calcium amount in the mix but strongly depends on its chemical nature.

Effect of calcium hydroxide addition

The addition of calcium hydroxide is detrimental for mechanical performances in binary (**Fig. 1**) and ternary mixtures, especially when its amount is superior to 5 wt.% (**Fig. 7**). These samples present a higher amount of portlandite than other formulations (**Fig. 4** and **Fig. 10**) and the addition of calcium hydroxide promotes the precipitation of CHc and hinders precipitation of hydrotalcite (**Fig. 3**). The high amount of portlandite is associated to a low dissolution of complementary calcium hydroxide, which is explained by a pH value of the pore solution superior to the equilibrium pH value of portlandite (12.5). Moreover, the common ion effect due to the high sodium concentration in the solution prevents calcium hydroxide dissolution [53]. The low dissolution of the complementary activator, along with the water addition due to the its use in a dry form, can result in a low concentration in activating ions in the solution, leading to a low extent of hydration. This assumption is supported by the presence of poorly hydrated slag grains noted by SEM (**Fig. 5**). The preferential precipitation of CHc over hydrotalcite is also associated to a lower extent of hydration [46] which explains the lower mechanical properties measured.

Effect of calcium sulfate addition

The addition of calcium sulfate is beneficial for mechanical properties when used with magnesium oxide in ternary mixture (**Fig. 7**). It is worth noting that the measured average compressive strength of this formulation (31.2 MPa) is close to the one measured on a sample of the same slag activated with pure sodium hydroxide in the same conditions and 10 wt.% of Na_2O (34.2 MPa) [46]. The partial

substitution of sodium hydroxide by calcium sulfate allows therefore to maintain equivalent mechanical properties while decreasing the sodium hydroxide amount needed. The presence of calcium sulfate hinders both CHc and hydrotalcite precipitation in favor of NS hydrates and calcite, whether in binary (**Fig. 3**) or ternary mixtures (**Fig. 9**). The aluminum dissolved from slag grains is then preferentially precipitated in sulfate than carbonate hydrates. Unlike the activation with sodium sulfate [24–26], no traces of ettringite have been found in these samples. This observation is attributed to the high pH value of the pore solution since ettringite is stable over the range of pH value between 10.7 and 13.0 [86]. It is worth noting that NS phase consumes a part of dissolved sodium which is no more available for slag dissolution nor integrated in C-(N)-A-S-H gel.

Effect of calcium carbonate addition

The addition of calcium carbonate enhances slag activation in binary and ternary mixtures. This is shown by the higher mechanical results (**Fig. 1** and **Fig. 7**) and the lower total and free water mass losses of the corresponding samples (**Fig. 4** and **Fig. 10**). Activation with calcium carbonate leads to the highest mechanical properties for binary (30.7 MPa) mixes and almost highest for ternary (30.4 MPa) mixtures. It does not seem to promote a specific phase precipitation when used in binary mixtures. However, calcium carbonate promotes hydrotalcite and prevents CHc precipitation when used in complement of magnesium oxide (**Fig. 10**), which is correlated to the development of higher mechanical properties (**Fig. 7**). Furthermore, these observations on the hydrates assemblage have been correlated, in a previous work [46], to a higher extent of hydration and was especially observed with Na_2O content superior or equal to 10 wt.% of slag mass. The combined use of calcium carbonate and magnesium oxide seems then to favor slag activation in a similar way than an increase in Na_2O content. These results are also promising in the objective of the reduction of the sodium hydroxide amount needed.

Effect of magnesium oxide addition

The use of magnesium oxide promotes the precipitation of hydrotalcite (**Fig. 4**). When MgO amount is increased to 5 wt.% of slag mass, the addition is detrimental for the mechanical strength because of the reduction in sodium concentration (-5%) due to the water addition needed to ensure a W/S of 0.4 as MgO is added in a dry state (**Table 3**). The extent of hydration is then reduced. This is observable by a higher amount of free water (**Fig. 4**) and the presence of anhydrous slag in the sample (**Fig. 5**).

The use of a calcic activator in addition to MgO in ternary mixes leads to similar or higher mechanical properties than the reference (**Fig. 7**). In this case, it is assumed that the calcic activator makes up for the decrease in sodium concentration and promotes a good dissolution, and thus activation, of the slag. This assumption is based on the high amount of hydrotalcite detected in these samples (**Fig. 10**) and on the dense hydrated microstructures observed by SEM (**Fig. 11**). The high amount of hydrotalcite precipitated, instead of CHc, has been correlated to a higher extent of hydration in a previous work [46].

Environmental impact

The results of the LCIA in terms of global warming potential (GWP) shows that all the binary mixtures present a lower impact than the NH_10 formulation (Fig. 12.a), which is one of the aims of this work. Especially, NH+CS and NH+Cc present an impact just slightly higher than the NH formulation (5 wt.%). This result lies on the fact that the CS and Cc production present the lowest GWP impact among the activators used (**Table 2**). However, the ternary mixtures contain MgO, which GWP impact is similar to that of NaOH (**Table 2**). Therefore, the GWP of the ternary mixtures are similar or even higher than the one of NH_10 formulation, especially in the case of NH+Mg+CH formulation which combines the relatively important impact of MgO and $Ca(OH)_2$ production (Fig. 12.a).

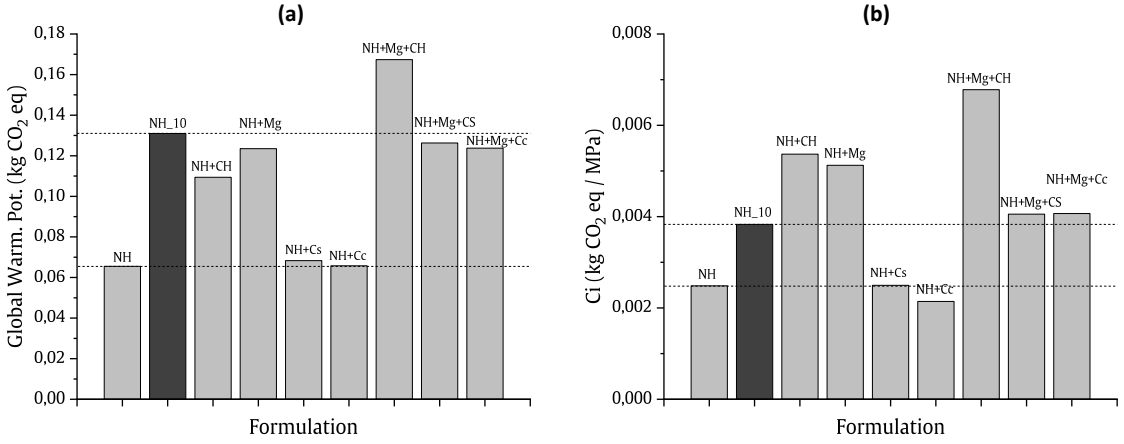

Fig. 12: (a) Global Warming Potential (kg CO_2 eq) and (b) CO_2 intensity (Ci) of the main formulations. The values are given for the activation of 1 kg of slag.

For comparison purpose among the formulations, we can consider the CO_2 intensity indicator (Ci) [4,87,88] and expressed as the amount of CO_2 emitted per functional unit, which is here the mechanical performance (**Fig. 1** and **Fig. 7**). The Ci of each formulation are given by (2):

$$Ci = \frac{GWP\ (kg\ CO_2 eq)}{Compressive\ Strength\ (MPa)} \quad (2)$$

It is worth noting that the Ci value for the NH_10 formulation is less than twice higher than the NH formulation (5 wt.%) (**Fig. 12**.b). It emphasizes the non-linear mechanical improvement achieved with increasing sodium hydroxide concentration [46].

Finally, only two formulations result in lower Ci than the NH_10 formulation: NH+CS and NH+Cc (**Fig. 12**.b). The NH+CS formulation presents a similar Ci to the NH formulation, so that the increase in GWP impact due to the addition of CS is balanced by an increase in compressive strength. Likewise, for the NH+Cc formulation, the mechanical performance improvement is higher than the GWP impact increase, resulting in a lower Ci value than the NH formulation. The NH+Mg+CS and NH+Mg+Cc formulations present similar Ci values than the NH_10 formulation. It underlines the fact that the mechanical improvement is not sufficient for these formulations to be interesting regarding NaOH substitution. Besides, three formulations present higher Ci values than the NH_10 formulation, especially due to the detrimental impact on compressive strength of $Ca(OH)_2$ and MgO additions (**Fig. 1** and **Fig. 7**).

In the same way that the CO_2 indicator, the environmental performance indicator (EPi) can be expressed for all the environmental indicators studied with (3):

$$EPi = \frac{Total\ Impact_i}{Compressive\ Strength\ (MPa)} \quad (3)$$

The Epi values (**Fig. 13**) allow to estimate the global environmental impact of a formulation which is not only focusing on the global warming potential impact. For comparison purpose, the Epi values of each indicator presented are normalized on the results obtained on all formulations. It mainly underlines that the use of high amount of sodium hydroxide (NH_10 formulation) has a non-negligible impact regarding fundamental issues such as Human Toxicity, Eutrophication or Ozone Layer depletion. The use of MgO and $Ca(OH)_2$ have also a relatively important impact regarding the majority of the indicators. Finally, the NH+Cc formulation present lower Epi values for all of the indicators.

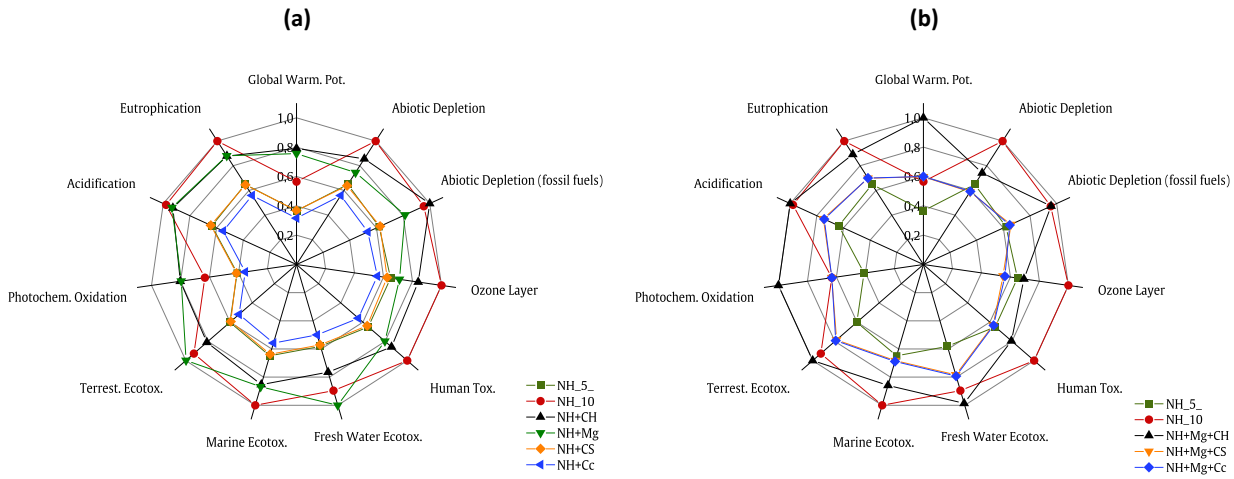

Fig. 13: Normalized EPi values obtained for each environmental indicator for (a) binary and (b) ternary mixtures.

5. Conclusion

Considering the results presented in this work the main following conclusions can be drawn:

- Slag activation is mainly driven by the concentration in sodium in the activating solution. Thus, it seems more appropriate to refer to the activators as their molar concentration in the solution rather than as their dry percentage of slag mass,
- The use of appropriate complementary activators, such as calcium carbonate (Cc) or calcium sulfate (CS), can help optimizing sodium hydroxide slag activation by increasing the extent of reaction and the mechanical properties (up to 18% with respect to a NaOH activation at 5 wt.%). The mechanical properties obtained were close to the one measured on the same slag with 10 wt.% of Na_2O, which is promising for a significant reduction of the sodium hydroxide content,
- The efficiency of the complementary activator used mainly relies on its chemical nature and its dissolution behavior in presence of highly concentrated sodium hydroxide solutions, which explains the positive effect of a Cc or Cs addition due to an increased solubility with alkali concentration. These results also underline the relevance of using complementary calcic activators to improve the mechanical performances,
- The nature and amount of the complementary activator impact the extent of hydration, the nature and the proportion of the hydrated phases,
- The use of Cc allows to achieve better environmental performances, regarding all the environmental indicators studied including the global warming potential impact. Those could be probably enhanced with an optimization of the NH/Cc weight ratio.

These conclusions support the efficiency and the relevance of using complementary activators to optimize slag hydration while enabling a partial decrease in sodium hydroxide content needed to trigger a satisfactory activation. A more significant range of complementary activators has to be studied with a larger range of addition amount to pursue the route of eco-efficient slag binders. The chemical interactions and dissolving behavior of the complementary activators with the highly alkaline activating solutions used to trigger slag hydration need to be also further investigated to better apprehend the efficiency of each activator and their role in slag activation and hydrates precipitation processes. The long-term mechanical performances and the durability in terms of carbonation, stability of hydrates or resistance to chemical attack and alkali leaching behavior of such activated slag should also be investigated.

6. References

[1] M. Abdulkareem, J. Havukainen, M. Horttanainen, How environmentally sustainable are fibre reinforced alkali-activated concretes?, J. Clean. Prod. 236 (2019). https://doi.org/10.1016/j.jclepro.2019.07.076.

[2] M. Abdulkareem, J. Havukainen, M. Horttanainen, Environmental Assessment of Alkali-Activated Mortars Using Different Activators, in: 17th Int. Waste Manag. Landfill Symp., CISA publisher, Italy, 2019. www.cisapublisher.com (accessed March 24, 2021).

[3] J.L. Provis, A. Palomo, C. Shi, Advances in understanding alkali-activated materials, Cem. Concr. Res. 78 (2015) 110–125.

[4] P.R. Cunningham, S.A. Miller, Quantitative Assessment of Alkali-Activated Materials: Environmental Impact and Property Assessments, J. Infrastruct. Syst. 26 (2020). https://doi.org/10.1061/(asce)is.1943-555x.0000556.

[5] M. Chi, Effects of dosage of alkali-activated solution and curing conditions on the properties and durability of alkali-activated slag concrete, Constr. Build. Mater. 35 (2012) 240–245. https://doi.org/10.1016/j.conbuildmat.2012.04.005.

[6] A. Fernández-Jiménez, J.G. Palomo, F. Puertas, Alkali-activated slag mortars Mechanical strength behaviour, Cem. Concr. Res. 29 (1999) 1313–1321.

[7] A. Fernández-Jiménez, F. Puertas, I. Sobrados, J. Sanz, Structure of Calcium Silicate Hydrates Formed in Alkaline-Activated Slag: Influence of the Type of Alkaline Activator, J. Am. Ceram. Soc. 86 (2003) 1389–94.

[8] C. Duran Atis ß, C. Bilim, Ç. Elik, O. Karahan, C. Duran Atis, C. Bilim, C., Elik, O. Karahan, Influence of activator on the strength and drying shrinkage of alkali-activated slag mortar, Constr. Build. Mater. 23 (2007) 548–555. https://doi.org/10.1016/j.conbuildmat.2007.10.011.

[9] G. Le Saoût, M. Ben Haha, F. Winnefeld, B. Lothenbach, Hydration degree of alkali-activated slags: A 29 Si NMR study, J. Am. Ceram. Soc. (2011). https://doi.org/10.1111/j.1551-2916.2011.04828.x.

[10] B. Walkley, R. San Nicolas, M.A. Sani, G.J. Rees, J. V. Hanna, J.S.J. van Deventer, J.L. Provis, Phase evolution of C-(N)-A-S-H/N-A-S-H gel blends investigated via alkali-activation of synthetic calcium aluminosilicate precursors, Cem. Concr. Res. 89 (2016) 120–135. https://doi.org/10.1016/j.cemconres.2016.08.010.

[11] M. Ben Haha, G. Le Saout, F. Winnefeld, B. Lothenbach, M. Ben Haha, G. Le Saout, F. Winnefeld, B. Lothenbach, Influence of activator type on hydration kinetics, hydrate assemblage and microstructural development of alkali activated blast-furnace slags, Cem. Concr. Res. 41 (2011) 301–310.

[12] A. Heath, K. Paine, M. Mcmanus, Minimising the global warming potential of clay based geopolymers, J. Clean. Prod. 78 (2014) 75–83. https://doi.org/10.1016/j.jclepro.2014.04.046.

[13] S. Song, D. Sohn, H.M. Jennings, T.O. Mason, Hydration of alkali-activated ground granulated blast furnace slag, J. Mater. Sci. 35 (2000) 249–257.

[14] G. Habert, J.B. D' Espinose De Lacaillerie, N. Roussel, An environmental evaluation of geopolymer based concrete production: Reviewing current research trends, J. Clean. Prod. (2011).

[15] R. Maddalena, J.J. Roberts, A. Hamilton, Can Portland cement be replaced by low-carbon alternative materials? A study on the thermal properties and carbon emissions of innovative cements, J. Clean. Prod. 186 (2018) 933–942. https://doi.org/10.1016/j.jclepro.2018.02.138.

[16] M. Weil, K. Dombrowski, A. Buchwald, Life-cycle analysis of geopolymers, in: J.L. Provis, J.S.J.B.T.-G. van Deventer (Eds.), Geopolymers. Struct. Process. Prop. Ind. Appl., Woodhead Publishing Series in Civil and Structural Engineering, Cambridge, UK, 2009: pp. 194–210. https://doi.org/https://doi.org/10.1533/9781845696382.2.194.

[17] K.C. Newlands, M. Foss, T. Matchei, J. Skibsted, D.E. Macphee, Early stage dissolution characteristics of aluminosilicate glasses with blast furnace slag-and fly-ash-like compositions, J. Am. Ceram. Soc. 100 (2017) 1941–1955. https://doi.org/10.1111/jace.14716.

[18] M. Fawer, M. Concannon, W. Rieber, Life Cycle Inventories for the Production of Sodium Silicates,

Int. J. Life Cycle Assess. 4 (1999) 207–212.
[19] X. Ke, S.A. Bernal, J.L. Provis, Controlling the reaction kinetics of sodium carbonate-activated slag cements using calcined layered double hydroxides, Cem. Concr. Res. 81 (2016) 24–37. https://doi.org/10.1016/j.cemconres.2015.11.012.
[20] A. Fernández-Jiménez, F. Puertas, Effect of activator mix on the hydration and strength behaviour of alkali-activated slag cements, Adv. Cem. Res. 15 (2003) 129–136.
[21] V. živica, Effects of type and dosage of alkaline activator and temperature on the properties of alkali-activated slag mixtures, Constr. Build. Mater. 21 (2007) 1463–1469. https://doi.org/10.1016/j.conbuildmat.2006.07.002.
[22] S.A. Bernal, R. San Nicolas, J.S. J van Deventer, J.L. Provis Professor, Alkali-activated slag cements produced with a blended sodium carbonate/sodium silicate activator, Adv. Cem. Res. 28 (2016) 262–273. https://doi.org/10.1680/jadcr.15.00013.
[23] F. Bellmann, J. Stark, Activation of blast furnace slag by a new method, Cem. Concr. Res. 39 (2009) 644–650.
[24] N. Mobasher, S.A. Bernal, J.L. Provis, Structural evolution of an alkali sulfate activated slag cement, J. Nucl. Mater. (2016). https://doi.org/10.1016/j.jnucmat.2015.11.016.
[25] A.M. Rashad, Y. Bai, P.A.M. Basheer, N.B. Milestone, N.C. Collier, Hydration and properties of sodium sulfate activated slag, Cem. Concr. Compos. (2013). https://doi.org/10.1016/j.cemconcomp.2012.12.010.
[26] Y. Zhao, J. Qiu, J. Xing, X. Sun, Chemical activation of binary slag cement with low carbon footprint, J. Clean. Prod. 267 (2020). https://doi.org/10.1016/j.jclepro.2020.121455.
[27] J. Alexandre, J.-L. Sebileau, Le Laitier de Haut Fourneau, C.T.P.L., Paris, France, 1988.
[28] G. Van Rompaey, Etude de la réactivité des ciments riches en laitier , à basse température et à temps court , sans ajout chloruré., Université Libre de Bruxelles Faculté, 2006.
[29] R. Dron, Mécanisme de la prise du laitier granulé sous activation alcaline, Laboratoire des Ponts et Chaussées. Ministère de l′ équipement, 1974.
[30] C. Houzé, Etude de la valorisation des laitiers de l′ industrie sidérurgique et de production des alliages silicomanganèse, Université Paris-Est, 2013.
[31] S. Kang, S.-A. Bak, K. Kim, M. Song, Properties of ion leaching of alkali-activated blast furnace slag at early hydration, Adv. Cem. Res. 28 (2016) 151–157. https://doi.org/10.1680/jadcr.15.00073.
[32] J.-P. Jolivet, De la solution à l′ oxyde. Condensation des cations en solution aqueuse. Chimie de surface des oxydes, InterEditions / CNRS Editions, Paris, France, 1994.
[33] F. Pacheco-Torgal, J.A. Labrincha, C. Leonelli, A. Palomo, P. Chindaprasirt, Handbook of alkali-activated cements, mortars and concretes, Woodhead P, Sawston, Royaume-Uni, Cambridge, Royaume-Uni, 2015.
[34] F.K. Crundwell, The mechanism of dissolution of minerals in acidic and alkaline solutions: Part II Application of a new theory to silicates, aluminosilicates and quartz, Hydrometallurgy. 149 (2014) 265–275. https://doi.org/10.1016/j.hydromet.2014.07.003.
[35] P. Krivenko, Why alkaline activation - 60 years of the theory and practice of alkali-activated materials, J. Ceram. Sci. Technol. 8 (2017) 323–333. https://doi.org/10.4416/JCST2017-00042.
[36] E. L ′hôpital, B. Lothenbach, K. Scrivener, D.A. Kulik, E. L′ Hôpital, B. Lothenbach, K. Scrivener, D.A. Kulik, E. L ′hôpital, B. Lothenbach, K. Scrivener, D.A. Kulik, Alkali uptake in calcium alumina silicate hydrate (C-A-S-H), Cem. Concr. Res. 85 (2016) 122–136. https://doi.org/10.1016/j.cemconres.2016.03.009.
[37] S.-Y. Hong, F.P. Glasser, Alkali binding in cement pastes Part I. The C-S-H phase, Cem. Concr. Res. 29 (1999) 1893–1903.
[38] I.G. Lodeiro, D.E. Macphee, A. Palomo, A. Fernández-Jiménez, Effect of alkalis on fresh C–S–H gels. FTIR analysis, Cem. Concr. Res. 39 (2009) 147–153. https://doi.org/10.1016/j.cemconres.2009.01.003.
[39] B. Lothenbach, A. Nonat, Calcium silicate hydrates: Solid and liquid phase composition, Cem. Concr. Res. 78 (2015) 57–70. https://doi.org/10.1016/j.cemconres.2015.03.019.

[40] B. Jönsson, H. Wennerström, Ion-Ion Correlations in Liquid Dispersions, J. Adhes. 80 (2004) 339–364. https://doi.org/10.1080/00218460490465551.
[41] C. Labbez, A. Nonat, I. Pochard, B. Jönsson, Experimental and theoretical evidence of overcharging of calcium silicate hydrate, J. Colloid Interface Sci. 309 (2007) 303–307. https://doi.org/10.1016/j.jcis.2007.02.048.
[42] S. Lesko, E. Lesniewska, A. Nonat, J.-C. Mutin, J.-P. Goudonnet, Investigation by atomic force microscopy of forces at the origin of cement cohesion, Ultramicroscopy. 86 (2001) 11–21.
[43] B. Jönsson, A. Nonat, C. Labbez, B. Cabane, H. Wennerström, Controlling the cohesion of cement paste, Langmuir. 21 (2005) 9211–9221. https://doi.org/10.1021/la051048z.
[44] C. Plassard, E. Lesniewska, I. Pochard, A. Nonat, Nanoscale Experimental Investigation of Particle Interactions at the Origin of the Cohesion of Cement, Am. Chem. Soc. (2005) 7263–7270.
[45] C. Labbez, B. Jönsson, I. Pochard, A. Nonat, B. Cabane, Surface Charge Density and Electrokinetic Potential of Highly Charged Minerals: Experiments and Monte Carlo Simulations on Calcium Silicate Hydrate, J. Phys. Chem. B. 110 (2006) 9219–9230. https://doi.org/10.1557/PROC-629-FF9.5.
[46] U. De Filippis, E. Prud′homme, S. Meille, Relation between Activator Ratio, Hydration Products and Mechanical Properties of Alkali-activated Slag, Constr. Build. Mater. 266 (2021). https://doi.org/10.1016/j.conbuildmat.2020.120940.
[47] F.K. Crundwell, The mechanism of dissolution of minerals in acidic and alkaline solutions: Part I-A new theory of non-oxidation dissolution, Hydrometallurgy. 149 (2014) 252–264. https://doi.org/10.1016/j.hydromet.2014.06.009.
[48] S.P. Newman, W. Jones, P. O′connor, D.N. Stamires, Synthesis of the 3R 2 polytype of a hydrotalcite-like mineral, J. Mater. Chem. 12 (2002) 153–155. https://doi.org/10.1039/b110715c.
[49] M. Ben Haha, B. Lothenbach, G. Le Saout, F. Winnefeld, Influence of slag chemistry on the hydration of alkali-activated blast-furnace slag – Part I: Effect of MgO, Cem. Concr. Res. 41 (2011) 955–963.
[50] Y. Yi, A. Al-Tabbaa, M. Liska, Properties and microstructure of GGBS-magnesia pastes, Adv. Cem. Res. 26 (2014) 114–122. https://doi.org/10.1680/adcr.13.00005.
[51] R.J. Myers, B. Lothenbach, S.A. Bernal, J.L. Provis, Thermodynamic modelling of alkali-activated slag cements, Appl. Geochemistry. 61 (2015) 233–247.
[52] R. Tänzer, A. Buchwald, D. Stephan, Effect of slag chemistry on the hydration of alkali-activated blast-furnace slag, Mater. Struct. 48 (2015) 629–641.
[53] P.W. Brown, The System Na20-Ca0-SiOrH20, J. Am. Ceram. Soc. 73 (1990) 3457–61. https://ceramics-onlinelibrary-wiley-com.docelec.insa-lyon.fr/doi/pdf/10.1111/j.1151-2916.1990.tb06475.x (accessed June 21, 2019).
[54] T. Santos, J. Almeida, J.D. Silvestre, P. Faria, Life cycle assessment of mortars: A review on technical potential and drawbacks, Constr. Build. Mater. 288 (2021). https://doi.org/10.1016/j.conbuildmat.2021.123069.
[55] G. Wernet, C. Bauer, B. Steubing, J. Reinhard, E. Moreno-Ruiz, B. Weidema, R. Zah, G. Wernet wernet, The ecoinvent database version 3 (part I): overview and methodology, Int J Life Cycle Assess. 21 (2016) 1218–1230. https://doi.org/10.1007/s11367-016-1087-8.
[56] G. Habert, C. Ouellet-Plamondon, Recent update on the environmental impact of geopolymers, RILEM Tech. Lett. 1 (2016) 17. https://doi.org/10.21809/rilemtechlett.v1.6.
[57] CML-IA Characterisation Factors, Leiden Univ. (2016). https://www.universiteitleiden.nl/en/research/research-output/science/cml-ia-characterisation-factors (accessed June 2, 2021).
[58] P.D. P. Kumar Mehta, P.D. Paulo J. M. Monteiro, Concrete: Microstructure, Properties, and Materials, Fourth Edition, 4th ed., McGraw-Hill Education, New York, 2014. https://www.accessengineeringlibrary.com/content/book/9780071797870.
[59] R. Ylmén, U. Jäglid, I. Panas, Monitoring Early Hydration of Cement by *Ex Situ* and *In Situ* ATR-FTIR - a Comparative Study, J. Am. Ceram. Soc. 97 (2014) 3669–3675.

https://doi.org/10.1111/jace.13186.
[60] T.L. Hughes, C.M. Methven, T.G.J. Jones, S.E. Pelham, P. Fletcher, C. Hall, Determining Cement Composition by Fourier Transform Infrared Spectroscopy, Adv. Cem. Based Mater. 2 (1995) 91–104.
[61] E. Kapeluszna, Ł. Kotwica, A. Różycka, Ł. Gołek, Incorporation of Al in C-A-S-H gels with various Ca/Si and Al/Si ratio: Microstructural and structural characteristics with DTA/TG, XRD, FTIR and TEM analysis, Constr. Build. Mater. 155 (2017) 643–653. https://doi.org/10.1016/j.conbuildmat.2017.08.091.
[62] H. Wijnja, C.P. Schulthess, ATR-FTIR and DRIFT spectroscopy of carbonate species at the aged k-Al 2 O 3 /water interface, Spectrochim. Acta Part A. 55 (1999) 861–872.
[63] Z.S. Nickolov, O. Ozcan, J.D. Miller, FTIR analysis of water structure and its significance in the flotation of sodium carbonate and sodium bicarbonate salts, Colloids Surfaces A Physicochem. Eng. Asp. 224 (2003) 231–239. https://doi.org/10.1016/S0927-7757(03)00317-0.
[64] V. Rives, S. Kannan, Layered double hydroxides with the hydrotalcite-type structure containing Cu 2+ , Ni 2+ and Al 3+, J. Mater. Chem. 10 (2000) 489–495.
[65] R.A. Buchanan, H.H. Caspers, J. Murphy, Lattice Vibration Spectra of Mg(OH)_2 and Ca(OH)_2, Appl. Opt. 2 (1963) 1147. https://doi.org/10.1364/ao.2.001147.
[66] M.B. Kruger, Q. Williams, R. Jeanloz, Vibrational spectra of Mg(OH)2 and Ca(OH)2 under pressure, J. Chem. Phys. 91 (1989) 5910–5915. https://doi.org/10.1063/1.457460.
[67] X. Zhu, X. Guo, J.R. Smyth, Y. Ye, X. Wang, D. Liu, High-Temperature Vibrational Spectra Between Mg (OH)2 and Mg (OD)2: Anharmonic Contribution to Thermodynamics and D/H Fractionation for Brucite, J. Geophys. Res. Solid Earth. 124 (2019) 8267–8280. https://doi.org/10.1029/2019JB017934.
[68] R. Ylmén, U. Jäglid, B.M. Steenari, I. Panas, Early hydration and setting of Portland cement monitored by IR, SEM and Vicat techniques, Cem. Concr. Res. 39 (2009) 433–439. https://doi.org/10.1016/j.cemconres.2009.01.017.
[69] M.Y.A. Mollah, W. Yu, R. Schennach, D.L. Cocke, A Fourier transform infrared spectroscopic investigation of the early hydration of Portland cement and the influence of sodium lignosulfonate, Cem. Concr. Res. 30 (2000) 267–273.
[70] M. Horgnies, J.J. Chen, C. Bouillon, Overview about the use of Fourier Transform Infrared spectroscopy to study cementitious materials, in: C.A. Brebbia, A. Klemm (Eds.), Mater. Characterisation VI. Comput. Methods Exp., WIT Press, Southampton, U.K, 2013: p. 364. https://doi.org/10.2495/MC130221.
[71] Y. Zuo, M. Nedeljković, G. Ye, Coupled thermodynamic modelling and experimental study of sodium hydroxide activated slag, Constr. Build. Mater. 188 (2018) 262–279. https://doi.org/10.1016/j.conbuildmat.2018.08.087.
[72] V.S. Ramachandran, R.M. Paroli, J.J. Beaudoin, A.H. Delgado, Handbook of Thermal Analysis of Construction Materials (Building Materials Series), William Andrew Publishing, Norwich, New, York, USA, 2002. https://doi.org/https://doi.org/10.1016/B978-081551487-9.50002-5.
[73] M. Sik Kim, Y. Jun, C. Lee, J. Eun Oh, Use of CaO as an activator for producing a price-competitive non-cement structural binder using ground granulated blast furnace slag, Cem. Concr. Res. 54 (2013) 208–214. https://doi.org/10.1016/j.cemconres.2013.09.011.
[74] W. Sha, Differential scanning calorimetry study of the hydration products in portland cement pastes with metakaolin replacement, Adv. Build. Technol. 1 (2007) 881–888. https://doi.org/10.1016/b978-008044100-9/50111-x.
[75] D. Nied, C. Stabler, M. Zajac, Assessing the Synergistic Effect of Limestone and Metakaolin, in: K. Scrivener (Ed.), Proc. 1st Int. Conf. Calcined Clays Sustain. Concr., Springer, 2015: pp. 245–251.
[76] A. Gruskovnjak, B. Lothenbach, L. Holzer, F. Winnefeld, Hydration of Alkali Activated Slag : Comparison with Ordinary Portland Cement, Adv. Cem. Res. 3 (2006) 119–128.
[77] S.-D. Wang, K.L. Scrivener, Hydration Products of Alkali Activated Slag Cement, Cem. End Concr. Res. 25 (1995) 561–571.

[78] K.J.D. Mackenzie, R.H. Meinhold, B.L. Sherriffb, Z. Xub, 27Al and 25Mg Solid-state Magic-angle Spinning Nuclear Magnetic Resonance Study of Hydrotalcite and its Thermal Decomposition Sequence, J. Mater. Chem. 3 (1993) 263.
[79] D.S. Klimesch, A. Ray, DTA-TGA evaluations of the CaO-Al2O3-SiO2-H2O system treated hydrothermally, Thermochim. Acta. 34 (1999) 115–122.
[80] K. Garbev, M. Bornefeld, G. Beuchle, P. Stemmermann, Cell dimensions and composition of nanocrystalline calcium silicate hydrate solid solutions. Part 2: X-ray and thermogravimetry study, J. Am. Ceram. Soc. 91 (2008) 3015–3023. https://doi.org/10.1111/j.1551-2916.2008.02601.x.
[81] A. Gruskovnjak, B. Lothenbach, F. Winnefeld, B. Münch, R. Figi, S.-C. Ko, M. Adler, U. Mäder, Quantification of hydration phases in supersulfated cements: review and new approaches, Adv. Cem. Res. 23 (2011) 265–275. https://doi.org/10.1680/adcr.2011.23.6.265.
[82] F.A. Miller, C.H. Wilkins, Infrared Spectra and Characteristic Frequencies of Inorganic Ions Their Use in Qualitative Analysis, Anal. Chem. 24 (1952) 1253–1294.
[83] M.A. Trezza, A.E. Lavat, Analysis of the system 3CaO.Al2O3 - CaSO4.2H2O - CaCO3 - H2O by FT-IR spectroscopy, Cem. Concr. Res. 31 (2001) 869–872.
[84] X.-Y. Peng, Y.-Y. Wang, L.-Y. Chai, Y.-D. Shu, Thermodynamic equilibrium of CaSO 4-Ca(OH) 2-H 2 O system, Trans. Nonferrous Met. Soc. China. 19 (2009) 249–252. https://doi.org/10.1016/S1003-6326(08)60260-5.
[85] E.J. Reardon, R. Fagan, The calcite/portlandite phase boundary: enhanced calcite solubility at high pH, Appl. Geochemistry. 15 (2000) 327–335.
[86] M. Medala, C. Labbez, I. Pochard, A. Nonat, Ettringite surface chemistry: Interplay of electrostatic and ion specificity, J. Colloid Interface Sci. 354 (2011) 765–770. https://doi.org/10.1016/j.jcis.2010.11.031.
[87] B.L. Damineli, F.M. Kemeid, P.S. Aguiar, V.M. John, Measuring the eco-efficiency of cement use, Cem. Concr. Compos. 32 (2010) 555–562. https://doi.org/10.1016/j.cemconcomp.2010.07.009.
[88] K.H. Yang, J.K. Song, K. Il Song, Assessment of CO 2 reduction of alkali-activated concrete, J. Clean. Prod. 39 (2013) 265–272. https://doi.org/10.1016/j.jclepro.2012.08.001.